Sensitivity-Enhanced NMR Techniques for the Study of Biomolecules

JOHN CAVANAGH and MARK RANCE

Department of Molecular Biology, The Scripps Research Institute, La Jolla, California 92037, USA

1. Introduction 2
2. General methodology 3
   2.1. Quadrature detection 3
   2.2. Cross-coil detection 4
   2.3. Principles of PEP technology 4
      2.3.1. The signal 5
      2.3.2. The noise 8
      2.3.3. Sensitivity improvement 9
      2.3.4. General comments 9
3. Sensitivity improvement in isotropic mixing (TOCSY) experiments 10
   3.1. Theory 12
   3.2. Experimental demonstration 13
      3.2.1. Mixing sequences 17
4. Sensitivity improvement in one-bond heteronuclear correlation experiments 18
   4.1. Theory 19
   4.2. Relaxation considerations 27
   4.3. Experimental demonstration 31
5. Sensitivity improvement in proton-detected two-dimensional heteronuclear relay spectroscopyx 36
   5.1. Theory 36
   5.2. Experimental demonstration 39
6. Sensitivity improvement in three-dimensional heteronuclear correlation spectroscopy 42
   6.1. 3D TOCSY–HMQC 42
   6.2. 3D NOESY–HMQC 44
   6.3. Experimental demonstration 46
7. Sensitivity improvement in proton-detected heteronuclear spin relaxation measurements 46
   7.1. Theory 48
   7.2. Experimental demonstration 51
8. Sensitivity enhancement in gradient-enhanced heteronuclear correlation spectroscopy 52

ANNUAL REPORTS ON NMR SPECTROCOPY
VOLUME 27 ISBN 0-12-505327-4

9. Additional applications 54
10. Conclusions 54
Acknowledgements 55
References 55

1. INTRODUCTION

Nuclear magnetic resonance spectroscopy is one of the most powerful tools available for obtaining detailed information on the structure, dynamics and interactions of molecules. Unfortunately, in comparison with some other physical methods, NMR spectroscopy is a relatively insensitive technique in terms of the achievable signal-to-noise ratio per unit measuring time. Indeed, in many applications of NMR spectroscopy, particularly to systems of biochemical interest, the inherent sensitivity of the measurements is a significant limiting factor in the quality and quantity of experimental information obtainable. Thus the optimization of the sensitivity of experimental measurements is an extremely important area of research and development in the application of NMR spectroscopy.

As indicated above, the term "sensitivity" in this chapter refers to the experimental signal-to-noise (S/N) ratio achievable for a given amount of measuring time. Many factors contribute to the sensitivity of an NMR experiment, and thus there are numerous ways in which the sensitivity potentially can be enhanced. These methods can generally be classified into three broad categories:

(i) optimization of experimental apparatus;

(ii) spin physics;

(iii) post-acquisition data processing.

In the first category are factors such as the magnetic field strength, sample volume and concentration and spectrometer design and performance.[1] The second category comprises of NMR techniques designed for achieving sensitivity improvements, such as polarization transfer experiments[2] and indirect detection methods.[3] Also included in the second category are factors directly concerning the acquisition of NMR data, such as optimum timing of experiments[4] and sampling of free induction decays.[5–7] The third category, post-acquisition data processing, covers areas such as optimum weighting,[4,5] apodization[8] and digital filtration of the recorded FID, and alternatives to Fourier transformation for spectral analysis.[9–11] The purpose of this chapter is not to review the very broad field of sensitivity enhancement in NMR spectroscopy, but rather to report on a specific class of new techniques for sensitivity improvement in multidimensional experiments which falls into the second category above.

The basic principle underlying this new class of sensitivity-enhanced NMR experiments is the preservation of spectral information that is normally discarded in the corresponding conventional experiments. When this additional information is combined in an appropriate fashion with the data normally collected, the composite data sets provide improvements in sensitivity over conventional experiments by factors of up to $\sqrt{2}$.

For convenience of discussion, this new methodology will be referred to as PEP (preservation of equivalent pathways). The theory underlying the basic concept is described in Section 2. Subsequent sections discuss the implementation of the sensitivity-improvement scheme in various types of solution-state multidimensional NMR experiments, with applications demonstrated on systems of biochemical interest.

2. GENERAL METHODOLOGY

The sensitivity-improvement scheme discussed here is closely related to that employed in quadrature phase-sensitive detection[12,13] and cross-coil detection[14] to achieve $\sqrt{2}$ improvements in sensitivity in 1D NMR spectroscopy. Thus, as an introduction to the PEP methodology, these analogous techniques will be discussed briefly.

2.1. Quadrature detection

Owing to the relatively high frequencies present in most NMR signals in pulsed Fourier transform spectroscopy, it is usually necessary to convert these signals to the audio frequency range before passing them to the analogue-to-digital converter. To do this frequency conversion, it is necessary to mix the NMR signal with a suitable reference source in a phase-sensitive detector[1,13] (most spectrometer designs employ at least a two-step frequency conversion process, but this is irrelevant for the present discussion). One problem with the use of a single phase-sensitive detector is that the sign of the converted NMR signal is not determined, i.e. frequencies equidistant above and below the reference source are indistinguishable.[12,13] One solution to this problem is to choose a frequency such that all the NMR signals are either above or below this reference. Unfortunately, this solution is disadvantageous for several reasons:

(i) the maximum sampling rate in the ADC process is twice what it might otherwise be;

(ii) since common source frequencies are usually necessary for the transmitter and receiver sections of the spectrometer, four times the RF power is required to compensate for the reference offset;

(iii) unless special precautions are taken, noise imaging will occur.

For the present discussion it is the latter point which is of particular relevance. Noise imaging occurs in a single phase-sensitive detector owing to the inability to distinguish the sign of the frequencies; if the noise at frequencies above and below the reference source is statistically independent then the noise imaging will degrade the achievable sensitivity by a factor of $\sqrt{2}$. Fortunately, the inability to distinguish between frequencies above and below the reference source in a single phase-sensitive detector can be overcome by employing two phase-sensitive detectors with reference sources that have identical frequencies but orthogonal phases.[12,13] The signals from the two detectors can then be combined as the real and imaginary parts of a complex function, which can be Fourier transformed to yield the desired spectrum with frequency sign discrimination. A $\sqrt{2}$ improvement in sensitivity will be realized as a result of the elimination of noise imaging, in addition to the advantages gained by placing the reference frequency in the middle of the spectral range of interest rather than at one end. Use of dual phase-sensitive detectors allows all of the information contained in the signal picked up by the probe coil to be recorded, resulting in substantial improvement in sensitivity.

2.2. Cross-coil detection

Hoult and co-workers[14] pointed out some time ago that, in principle, a $\sqrt{2}$ improvement in sensitivity could be achieved through the use of two orthogonal detection coils; this improvement is in addition to that discussed above for quadrature phase-sensitive detection employing a single coil. The concept is very simple. If the two coils are orthogonally situated but otherwise identical, the NMR signals detected by them will be identical except for a relative 90° phase shift; on the other hand, the thermal noise in the receiver circuits (probe coil plus preamplifiers) will be uncorrelated. Therefore, when the signals from the two coils are combined after correcting for the relative phase shift, the coherent NMR signals will double in intensity while the noise level will only increase by $\sqrt{2}$, resulting in a net increase of $\sqrt{2}$ in sensitivity over a single-coil detection system.

2.3. Principles of PEP technology

The PEP technique is essentially an analogue of cross-coil detection for evolution periods[8] in multidimensional experiments. To illustrate the basic principle, the effect of the simple three-pulse sequence:

$$90^\circ_\beta\text{–}t_1\text{–}90^\circ_x\text{–}90^\circ_\phi\text{–}t_2 \quad \text{(detection)}$$

on an isolated spin ½ will be analysed.

2.3.1. The signal

Starting at thermal equilibrium, the net magnetization of the spin ½ is proportional to the z component of its angular momentum, I_z. The first 90° pulse rotates the magnetization to the transverse plane, and the subsequent evolution period results in the following density operator (assuming $\beta = y$ and ignoring constants of proportionality):

$$\sigma_y(t_1) = I_x \cos \Omega t_1 + I_y \sin \Omega t_1, \tag{1}$$

where Ω is the resonance offset in the rotating frame. The third 90° pulse is phase-cycled such that the pulse pair 90°_x–90°_ϕ results in net rotations of 0° ($\phi = -x$) or 180° ($\phi = x$) about the x axis. Thus, after the pulse pair, the density operator is given by

$$\sigma_y^{-x}(t_1) = I_x \cos \Omega t_1 + I_y \sin \Omega t_1 \tag{2a}$$

for $\phi = -x$ and

$$\sigma_y^{x}(t_1) = I_x \cos \Omega t_1 - I_y \sin \Omega t_1 \tag{2b}$$

for $\phi = x$. Subsequent evolution during the t_2 detection period of this simple 2D experiment results in the following density operators:

$$\begin{aligned}\sigma_y^{-x}(t_1, t_2) = {} & I_x(\cos \Omega t_1 \cos \Omega t_2 - \sin \Omega t_1 \sin \Omega t_2) \\ & + I_y (\sin \Omega t_1 \cos \Omega t_2 + \cos \Omega t_1 \sin \Omega t_2),\end{aligned} \tag{3a}$$

$$\begin{aligned}\sigma_y^{x}(t_1, t_2) = {} & I_x(\cos \Omega t_1 \cos \Omega t_2 + \sin \Omega t_1 \sin \Omega t_2) \\ & - I_y(\sin \Omega t_1 \cos \Omega t_2 - \cos \Omega t_1 \sin \Omega t_2).\end{aligned} \tag{3b}$$

These expressions can be rewritten as

$$f_y^{-x}(t_1, t_2) = \exp(\mathrm{i}\Omega t_1) \exp(\mathrm{i}\Omega t_2), \tag{4a}$$

$$f_y^{x}(t_1, t_2) = \exp(-\mathrm{i}\Omega t_1) \exp(\mathrm{i}\Omega t_2), \tag{4b}$$

where the real and imaginary components correspond to the I_x and I_y coefficients respectively. A two-dimensional Fourier transformation[8] of the signals represented by (4) (with appropriate damping factors included), will result in 2D spectra with a single resonance at frequencies $\omega_1 = \Omega(\phi = -x)$ or $\omega_1 = -\Omega(\phi = x)$ and $\omega_2 = \Omega$; unfortunately, this resonance will have a highly undesirable, mixed lineshape.[15,16] This phase-twisted lineshape results from the phase modulation with respect to t_1 of the detected NMR signal. As discussed by Keeler and Neuhaus,[16] pure absorption lineshapes can be obtained by converting the phase-modulated signal to an amplitude-modulated signal. In the example discussed here this can be accomplished by adding (or subtracting) the signals represented by (2). Adding the operators yields

$$\sigma_y^{a}(t_1) = 2I_x \cos \Omega t_1 \tag{5}$$

or

$$f_y^a(t_1, t_2) = 2 \cos \Omega t_1 \exp(i\Omega t_2), \tag{6}$$

while subtraction yields

$$\sigma_y^s(t_1) = 2I_y \sin \Omega t_1 \tag{7}$$

or

$$f_y^s(t_1, t_2) = 2i \sin \Omega t_1 \exp(i\Omega t_2). \tag{8}$$

When the signal $f_y^a(t_1, t_2)$ in (6) is subjected to a cosine Fourier transformation with respect to t_1 and a complex Fourier transformation with respect to t_2, a resonance with a pure absorption lineshape in both frequency dimensions of the 2D spectrum will be observed; likewise, if $f_y^s(t_1, t_2)$ in (8) is subjected to a sine Fourier transformation with respect to t_1 and a complex Fourier transformation with respect to t_2, an identical double absorption resonance will be observed. If the transformed spectra are added together, the resonance will double in intensity.

In conventional experiments only one of the signals, either addition or subtraction, is retained; the phase cycling of the RF pulses and receiver is engineered such that only one combination is accumulated in computer memory, i.e. the signal arising from only one of the orthogonal magnetization components present during t_1 is retained. However, it is clear from the discussion that retention of either component and use of appropriate data processing leads to identical spectra, in the absence of noise and pulse imperfections, which can be combined to enhance the signal. The key to the PEP technique is the behaviour of the spectral noise when the data are combined to enhance the signal; this issue will be discussed below.

Before proceeding to the discussion of noise, the analysis of the coherent signal behaviour will be extended somewhat for the sake of generality. In the procedure outlined above, a phase-modulated signal, for example (4a), is converted to an amplitude-modulated signal, for example (6). This process results in the loss of the ability to distinguish the sign of the resonance frequency in the ω_1 dimension. As discussed by Keeler and Neuhaus,[16] there are at least two related procedures for recovering the ability for ω_1 sign discrimination: (i) the so-called hypercomplex method,[17] also commonly referred to as the States method,[18] and (ii) the time-proportional phase-incrementation technique (TPPI).[19–21] For ease of discussion, the hypercomplex method for ω_1 sign discrimination will be included in the present example. If one considers the additive combination of the data for the two phase steps ($\phi = \pm x$) in the present example, the signal during the detection period is given by (6). If the experiment is repeated with the phase of the first pulse advanced by 90°, the corresponding signal during the detection period is

$$f_{-x}^a(t_1, t_2) = -2 \sin \Omega t_1 \exp(i\Omega t_2). \tag{9}$$

The signals in the two experiments, (6) and (9), can be combined as complex pairs with respect to t_1, and a complex Fourier transformation will yield an absorptive resonance with sign discrimination in the ω_1 dimension. If one considers the subtractive combination for the two phase steps ($\phi = \pm x$) with $\beta = -x$, the detected signal is

$$f^{s}_{-x}(t_1, t_2) = 2i \cos \Omega t_1 \exp(i\Omega t_2). \tag{10}$$

As for the case of the additive combination, (8) and (10) can be combined as complex pairs with respect to t_1, and a complex Fourier transformation performed to yield the desired spectral information.

The discussion above focused on the additive, (6) and (9), and subtractive, (8) and (10), data sets being processed separately and combined only at the end as 2D spectra to enhance the NMR resonance intensity. In practice, it is much simpler to combine the time domain data sets so that a single 2D Fourier transformation is required. Inspection of (6), (8), (9) and (10) indicates that the time domain data should be combined as follows:

$$f^{r}(t_1, t_2) = f^{a}_{y}(t_1, t_2) - i f^{s}_{-x}(t_1, t_2) \tag{11}$$

$$= 4 \cos \Omega t_1 \exp(i\Omega t_2) \tag{12}$$

$$f^{i}(t_1, t_2) = f^{a}_{-x}(t_1, t_2) + i f^{s}_{y}(t_1, t_2) \tag{13}$$

$$= -4 \sin \Omega t_1 \exp(i\Omega t_2). \tag{14}$$

The superscripts r and i indicate that these functions should be combined as complex pairs with respect to t_1 in the usual hypercomplex prescription[16–18] prior to the complex ω_1 Fourier transformation; a complex Fourier transformation with respect to t_2 should be performed separately on (11) and (13). The factor i in the second term of (11) indicates that the real and imaginary components of $f^{s}_{-x}(t_1, t_2)$ should be interchanged and one component negated[22] before being combined with $f^{a}_{y}(t_1, t_2)$; a similar operation is indicated in (13).

The signal enhancement in the PEP technique is clearly demonstrated in the analysis above. In a conventional experiment only the additive (or subtractive) combination of the two-step phase cycle ($\phi = \pm x$) would be accumulated, leading to the signals of (6) and (9) (or (8) and (10)); with the PEP technique, information from equivalent pathways is preserved and combined appropriately to double the signal intensity, as indicated in (12) and (14). It should be emphasized that this signal enhancement is achieved without any additional data being recorded. In conventional experiments the signal arising from only one of the two orthogonal transverse magnetization components present during the mixing time is retained, while in the PEP technique the signals from both transverse components, which contain equivalent spectral information, are preserved, in direct analogy to cross-coil detection in 1D spectroscopy.

2.3.2. *The noise*

The straightforward analysis presented above has indicated that the NMR signal intensity for a given experimental acquisition time can be doubled through the use of the PEP methodology. The key, therefore, to determining the sensitivity of the technique is the behaviour of the spectral noise. In the original description of the PEP technology[23] it was demonstrated via an analysis of the frequency domain spectra that the spectral noise increased by a factor of $\sqrt{2}$ in the enhanced spectra relative to the conventional spectra. An equivalent proof is provided here based on a simple inspection of the time domain data.

To determine the noise behaviour, it is sufficient to consider the data accumulated for a single value of t_1. In the example introduced above, four free induction decays are recorded and stored separately, corresponding to the two-step phase cycle ϕ and the two steps ($\beta = y, =x$) required for ω_1 sign discrimination. These four free induction decays can be designated as

$$F_y^x(t_2) = [\mathrm{Fr}]_y^x(t_2) + \mathrm{i}[\mathrm{Fi}]_y^x(t_2) \tag{15}$$

$$F_y^{-x}(t_2) = [\mathrm{Fr}]_y^{-x}(t_2) + \mathrm{i}[\mathrm{Fi}]_y^{-x}(t_2) \tag{16}$$

$$F_{-x}^x(t_2) = [\mathrm{Fr}]_{-x}^x(t_2) + \mathrm{i}[\mathrm{Fi}]_{-x}^x(t_2) \tag{17}$$

$$F_{-x}^{-x}(t_2) = [\mathrm{Fr}]_{-x}^{-x}(t_2) + \mathrm{i}[\mathrm{Fi}]_{-x}^{-x}(t_2) \tag{18}$$

where the superscripts refer to the phase ϕ, the subscripts to the phase β, and the Fr and Fi refer to the real and imaginary components of the free induction decays respectively. The additive combination of the free induction decays for the phase cycle ϕ are

$$\begin{aligned} F_y^{\mathrm{a}} &= F_y^x + F_y^{-x} \\ &= ([\mathrm{Fr}]_y^x + [\mathrm{Fr}]_y^{-x}) + \mathrm{i}([\mathrm{Fi}]_y^x + [\mathrm{Fi}]_y^{-x}), \end{aligned} \tag{19}$$

$$\begin{aligned} F_{-x}^{\mathrm{a}} &= F_{-x}^x + F_{-x}^{-x} \\ &= ([\mathrm{Fr}]_{-x}^x + [\mathrm{Fr}]_{-x}^{-x}) + \mathrm{i}([\mathrm{Fi}]_{-x}^x + [\mathrm{Fi}]_{-x}^{-x}) \end{aligned} \tag{20}$$

where the explicit reference to t_2 has been omitted for convenience. The subtractive combinations are

$$\begin{aligned} F_y^{\mathrm{s}} &= F_y^x - F_y^{-x} \\ &= ([\mathrm{Fr}]_y^x - [\mathrm{Fr}]_y^{-x}) + \mathrm{i}([\mathrm{Fi}]_y^x - [\mathrm{Fi}]_y^{-x}), \end{aligned} \tag{21}$$

$$\begin{aligned} F_{-x}^{\mathrm{s}} &= F_{-x}^x - F_{-x}^{-x} \\ &= ([\mathrm{Fr}]_{-x}^x - [\mathrm{Fr}]_{-x}^{-x}) + \mathrm{i}([\mathrm{Fi}]_{-x}^x - [\mathrm{Fi}]_{-x}^{-x}). \end{aligned} \tag{22}$$

Following the prescription outlined above for combining the additive and subtractive data sets, the composite time domain data are specified by

$$F_y^c = F_y^a - iF_{-x}^s, \tag{23}$$

$$F_{-x}^c = F_{-x}^a + iF_y^s. \tag{24}$$

Substituting (19–22) into (23) and (24) leads to

$$F_y^c = ([Fr]_y^x + [Fr]_y^{-x} + [Fi]_{-x}^x - [Fi]_{-x}^{-x}) + i([Fi]_y^x + [Fi]_y^{-x} - [Fr]_{-x}^x + [Fr]_{-x}^{-x}), \tag{25}$$

$$F_{-x}^c = ([Fr]_{-x}^x + [Fr]_{-x}^{-x} - [Fi]_y^x + [Fi]_y^{-x}) + i([Fi]_{-x}^x + [Fi]_{-x}^{-x} + [Fr]_y^x - [Fr]_y^{-x}). \tag{26}$$

The real and imaginary components of F_y^c and F_{-x}^c are each the sum of four statistically independent data sets (it is assumed for the present analysis that the free induction decays in (19)–(22) consist simply of random noise), whereas the additive data set, (19) and (20), and the subtractive data set, (21) and (22), are each the sum of only two statistically independent data sets. Therefore, since random noise increases by $n^{1/2}$ when n independent noise samples are combined, the composite data set represented by (25) and (26) will have a noise level $\sqrt{2}$ larger than either the additive or subtractive data sets in (19)–(22).

2.3.3. Sensitivity improvement

The analysis in Section 2.3.1 demonstrated that the NMR signal intensity in the example experiment could be doubled by making an appropriate combination of the data accumulated separately for distinct phase steps in the pulse sequence. In Section 2.3.2 it was demonstrated that the prescription for the combination of data that leads to the doubling of NMR intensities results in a $\sqrt{2}$ increase in noise compared to the conventional data set. Thus the net improvement in the signal-to-noise ratio is a factor of $\sqrt{2}$. Since this improvement is achieved with no increase in the experimental acquisition time, a significant sensitivity enhancement is realized.

2.3.4. General comments

The analysis presented above for a simple experiment was sufficient to demonstrate the general principle upon which the PEP methodology is based. By recording separately the data for phase-cycling steps normally incorporated to suppress one of the orthogonal transverse magnetization components during an evolution period of a multidimensional experiment, it is possible to obtain separate spectra from signals arising from the two components. If the nature of the experiment is such that the two spectra are

essentially equivalent, the spectra can be combined to achieve an improvement in sensitivity up to $\sqrt{2}$. This will be the case if the two transverse magnetization components are subjected to the same mixing process between the evolution and detection periods. In the simple example provided above the mixing process consisted only of a pair of 90° pulses. Strictly speaking, the mixing process was not identical for the two transverse magnetization components, since one was spin-locked along the rotation axis of the pulses while the other was being rotated. However, neglecting significant pulse imperfections and off-resonance effects, the two magnetization components could be treated, to a good approximation, as though they had experienced the same mixing processs. An example in which the process would be quite different for the two orthogonal magnetization components is a 2D NOESY experiment;[24] the pulse sequence is the same as above except that a finite mixing time τ_m is inserted between the second and third 90° pulses. In this case one of the transverse components during the evolution period will be rotated to the longitudinal axis during the mixing time, while the other will remain in the transverse plane; clearly, the coherent and relaxation behaviours of these two components during τ_m will be quite different, and the resulting spectra will not be equivalent.

In the following sections the application of PEP technology to various types of multidimensional NMR experiments will be described. The element in common to all of these experiments is that the mixing process essentially treats equally the two orthogonal transverse magnetization components present during an evolution period, so that if the NMR signals arising from both these components are retained, a sensitivity improvement can be achieved.

3. SENSITIVITY IMPROVEMENT IN ISOTROPIC MIXING (TOCSY) EXPERIMENTS

One of the most popular techniques currently employed for obtaining resonance assignments in high resolution ^{1}H NMR spectroscopy is the TOCSY experiment (sometimes referred to as HOHAHA).[25,26] In this experiment magnetization is transferred coherently from one spin to another belonging to the same scalar-coupled spin system during an extended mixing period. During this mixing period some RF pulse sequence is applied that, ideally, eliminates the chemical-shift terms from the nuclear spin Hamiltonian and leaves only the isotropic scalar coupling interactions. The TOCSY experiment derives its popularity from several advantages:

(i) coherence transfer through a spin system is a continuous process, allowing correlations to be established through an extended coupling network, subject to favourable relaxation rates;

(ii) a net transfer of magnetization is achieved more rapidly than via alternative, pulse-interrupted free precession techniques;

(iii) with a suitable implementation of the TOCSY experiment,[26–28] the spectra obtained have resonances with predominantly absorption lineshapes.

It is important to note that a net transfer of magnetization gives rise to NMR resonances for which the multiplet components are all in phase (i.e. have the same algebraic sign). This is a very advantageous feature in cases where the linewidth exceeds the size of the active scalar couplings, since then the antiphase multiplets are severely attenuated owing to the destructive interference of the antiphase multiplet components. Thus the TOCSY experiment is particularly useful in cases where the resonance linewidths are large because of molecular size or exchange effects.

The general scheme for the most flexible version of the 2D TOCSY experiment is[27,28]

$$\text{(equilibration)–90°–}t_1\text{–90°–(isotropic mixing)–90°–}t_2\text{(acquire)}.$$

During the t_1 evolution period the initial transverse magnetization created by the first 90° pulse evolves under the influence of both chemical-shift and scalar coupling interactions. At the end of the evolution period another 90° pulse prepares the system to enter the subsequent isotropic mixing period. The mixing period consists of a multipulse sequence designed to eliminate chemical-shift terms and give rise to a nuclear spin Hamiltonian consisting of only the isotropic scalar coupling terms. During the mixing period, magnetization is coherently transferred among spins belonging to the same coupling network. At the end of the mixing, a third 90° pulse generates the appropriate transverse magnetization to be detected, and the data are processed to provide a 2D correlation map. Any arbitrary coherence can be transferred under the isotropic mixing process to another of the same order; however, it is most common to focus on the transfer of net magnetization, $M_{i\phi} \rightarrow M_{j\phi}$($\phi = x$, y or z, and i and j are any two spins belonging to the same spin system), since all other coherences or multispin order will give rise to resonances that have antiphase multiplet structure. While such antiphase contributions can be observed in TOCSY spectra as distortions of the otherwise in-phase multiplet structures, their contribution is usually minimal owing to the destructive interference of the antiphase multiplet components, especially when the resonance linewidths are comparable to the active scalar couplings. This is very often the case in the study of large biomolecules. For this reason, the analysis here will focus on only the single spin order terms and those single quantum coherences that lead to resonances with in-phase multiplet structure.

3.1. Theory

To understand the origin of the sensitivity improvement in the TOCSY experiment,[23] it is sufficient to consider the behaviour of a weakly coupled two-spin system AX. The nuclear spin angular momentum operators for the spins A and X are denoted by I_ϕ and S_ϕ respectively, where $\phi = x$, y or z. At the end of the evolution period the density matrix will be given by (ignoring constants of proportionality and all relaxation effects)[29–31]

$$\begin{aligned}\rho(t_1) = & -I_y \cos \Omega_A t_1 \cos \pi J t_1 + 2I_x S_z \cos \Omega_A t_1 \sin \pi J t_1 \\ & + I_x \sin \Omega_A t_1 \cos \pi J t_1 + 2I_y S_z \sin \Omega_A t_1 \sin \pi J t_1 \\ & + \text{similar terms with } I \text{ and } \Omega_A \text{ replaced by } S \text{ and } \Omega_X, \end{aligned} \tag{27}$$

where J is the scalar coupling between A and X; Ω_A and Ω_X are the resonance offsets of spins A and X, and the first 90° pulse is assumed to have phase x. For convenience the terms with transverse S_ϕ components will be omitted. The two-spin terms in (27) will give rise to peaks that have antiphase multiplet structure in the ω_1 dimension of the 2D TOCSY spectrum and a mixture of both in-phase and antiphase character in the ω_2 dimension. For the reasons stated above, all antiphase contributions will be ignored in the present discussion, so that (27) simplifies to

$$\rho(t_1) = -I_y \cos \Omega_A t_1 \cos \pi J t_1 + I_x \sin \Omega_A t_1 \cos \pi J t_1. \tag{28}$$

A subsequent 90° pulse of phase x generates the terms

$$\rho(t_1, 90_x) = -I_z \cos \Omega_A t_1 \cos \pi J t_1 + I_x \sin \Omega_A t_1 \cos \pi J t_1. \tag{29}$$

Assuming that the effective nuclear spin Hamiltonian during the ensuing mixing period consists only of the isotropic scalar coupling term $2\pi \boldsymbol{I} \cdot \boldsymbol{S}$, the density matrix at the end of the mixing period τ will be given by[25]

$$\begin{aligned}\rho(t_1, 90_x, \tau) = & -I_z \cos \Omega_A t_1 \cos \pi J t_1 \cos \pi J \tau + I_x \sin \Omega_A t_1 \cos \pi J t_1 \cos \pi J \tau \\ & - S_z \cos \Omega_A t_1 \cos \pi J t_1 \sin \pi J \tau + S_x \sin \Omega_A t_1 \cos \pi J t_1 \sin \pi J \tau \\ & + \text{antiphase terms.} \end{aligned} \tag{30}$$

The antiphase terms are ignored, since they give rise to antiphase contributions in the final spectrum. The final 90° pulse of phase x then generates the following observable magnetization:

$$\begin{aligned}\rho(t_1, 90_x, \tau, 90_x) = & I_y \cos \Omega_A t_1 \cos \pi J t_1 \cos \pi J \tau \\ & + I_x \sin \Omega_A t_1 \cos \pi J t_1 \cos \pi J \tau \\ & + S_y \cos \Omega_A t_1 \cos \pi J t_1 \sin \pi J \tau \\ & + S_x \sin \Omega_A t_1 \cos \pi J t_1 \sin \pi J \tau. \end{aligned} \tag{31}$$

When the resulting NMR signal is detected during the t_2 period and subjected to 2D Fourier transformation, a diagonal peak for the I spin and a cross-peak to the S spin will be observed, as well as the diagonal peak for

the S spin and cross-peak to the I spin from terms that were dropped earlier. The lineshapes for all these peaks will be the highly undesirable phase twist, a mixture of two-dimensional absorption and dispersion. In order to obtain absorption mode spectra in the version of the TOCSY experiment described, one of the orthogonal components in (31) is removed by the use of phase cycling.[27] In other variants of the TOCSY experiment[26] RF field inhomogeneity ("trim" pulse) is used for the same purpose; sensitivity improvement via PEP technology is not possible in this case, since one of the necessary orthogonal magnetization components is destroyed.

Unlike many experiments, where the desired spectral information is obtained through a unique pathway, the isotropic mixing experiment allows equivalent information to be obtained simultaneously along two orthogonal axes. As noted above, the key to sensitivity improvement is to employ the PEP technology to retain the information obtained along both orthogonal axes and combine it in such a way that pure 2D absorption lineshapes result.

If the phase of the 90° pulse immediately prior to the isotropic mixing period is inverted i.e. changed from x to $-x$, the signal eventually detected evolves from the following density operator at the beginning of the t_2 period:

$$\begin{aligned}\rho(t_1, 90_{-x}, \tau, 90_x) = & -I_y \cos \Omega_A t_1 \cos \pi J t_1 \cos \pi J \tau \\ & + I_x \sin \Omega_A t_1 \cos \pi J t_1 \cos \pi J \tau \\ & - S_y \cos \Omega_A t_1 \cos \pi J t_1 \sin \pi J \tau \\ & + S_x \sin \Omega_A t_1 \cos \pi J t_1 \sin \pi J \tau. \end{aligned} \tag{32}$$

Rather than combining the two data sets represented by (31) and (32) in real time as the experiment proceeds, the data can be stored separately ready for combination later. By adding (31) and (32), only the I_x components are retained, while the difference retains only the I_y components. Ideally the two spectra that result will be identical except for a 90° phase shift in both dimensions. Thus, once the two spectra are each phased to give pure 2D absorption lineshapes, they can be co-added to double the size of all peaks. As shown above, in the PEP method, the noise from the two spectra combines as though statistically independent, giving an overall sensitivity improvement of $\sqrt{2}$ compared with the conventional method. The data can also be combined in the time domain, as discussed in Section 2.3, if the hypercomplex method has been employed for ω_1 frequency discrimination.

3.2. Experimental demonstration

Before proceeding with the experimental demonstration of the sensitivity-enhanced TOCSY procedure, it is important to note that there is an alternate method in which the data can be treated. From (31) and (32) it can be seen that the two orthogonal magnetization components M_x and M_y (which are proportional to I_x and I_y respectively) have sine and cosine

amplitude modulations respectively as functions of t_1. Thus these separated components may be combined in the manner referred to as the hypercomplex method to discriminate the signs of the ω_1 frequencies.[17,18] It can be demonstrated that the hypercomplex combination will result in a spectrum with the same signal-to-noise ratio as a spectrum obtained in the conventional way, where the orthogonal components are recorded in two separate experiments by phase-shifting the first 90° pulse by 90°. Since the modified experiment is completed in half the time of the conventional method (N scans per t_1 in the modified experiment versus $2N$ scans in the conventional experiment), a gain in sensitivity of $\sqrt{2}$ is realized. The drawback of the hypercomplex implementation of the sensitivity-improved experiment is that if the two quadrature magnetization components do not have exactly the same amplitude then ω_1 quadrature images will appear in the 2D TOCSY spectra. Owing to non-idealities in the mixing sequence, there will likely be some small amplitude differences in the orthogonal components, and so this implementation of the sensitivity improvement is not recommended. The conventional hypercomplex method for ω_1 quadrature detection can still be employed with the scheme described above for combining separate spectra to obtain the sensitivity improvement.

For the z-filtered TOCSY experiment[27,28] employed here the general scheme can be written as

$$\text{(equilibration)}\text{–}90^\circ_{\phi+\beta+\psi}\text{–}t_1\text{–}90^\circ_{\varepsilon}\text{–(mixing)}_{\gamma}\text{–}90^\circ_{\alpha}\text{–}t_2\text{(acq, rec} = \alpha + \beta).$$

At the end of the t_1 period, one of the orthogonal transverse in-phase magnetization components is rotated to the z axis by the pulse immediately preceding the mixing period. In the conventional z-filtered TOCSY experiment $\phi = \varepsilon$, and the first two 90° pulses are phase-cycled (i.e. ϕ and ε are advanced in increments of 90°) to eliminate the remaining transverse single-quantum components as well as higher-order coherences. For axial peak suppression $\beta = 0°$, 180°, and ψ is incremented to obtain ω_1 sign discrimination. In the modification proposed here two data sets are recorded; in both data sets the phase cycling of β and ψ is unchanged, but the remaining cycling is such that $\phi = \alpha$ is incremented in steps of 90° simply to remove ω_2 quadrature images and $\gamma = \phi + 90°$ for mixing sequences such as WALTZ[32] and DIPSI[33] (see below). The difference in the two acquisitions is that in one $\varepsilon = \phi$, while in the other $\varepsilon = \phi + 180°$. The result will be that the z component of the magnetization during the mixing period will be inverted between the two experiments, while the transverse component will be unaffected; thus addition and subtraction of the data sets will allow these two components to be separated. While the restricted phase cycling will not eliminate higher-order coherences, the contributions from these terms are minimal.

To show that virtually identical spectra can be obtained from the coherence pathways selecting the two orthogonal magnetization components

M_x and M_z during the mixing time, 2D TOCSY spectra were obtained for a 1 mM solution (D_2O) of the protein bovine pancreatic trypsin inhibitor (pD 4.7, 303 K). The mixing time was 69 ms; this value was chosen to enhance long-range coherence transfer.[34] The spectra were obtained at 500 MHz on a Bruker AM500 spectrometer using the modified z-filtered sequence and phase cycling described above. More explicitly, the basic phase cycling used was as follows:

For the first experiment: 1st 90° pulse: $+x$, $-x$; 2nd 90° pulse: $+x$, $+x$; mixing sequence: $+y$, $+y$; 3rd 90° pulse: $+x$, $+x$; receiver: $+x$, $-x$.

For the second experiment: 1st 90° pulse: $+x$, $-x$; 2nd 90° pulse: $-x$, $-x$; mixing sequence: $+y$, $+y$; 3rd 90° pulse: $+x$, $+x$; receiver: $+x$, $-x$.

Note the only change is the inversion of the second pulse. Furthermore, all phases were advanced in increments of 90° to eliminate quadrature images in the acquisition dimension, to give a total of eight steps for the complete phase cycle in each experiment. The TPPI scheme[21] was used for sign discrimination of the ω_1 frequencies. Although it is unnecessary in the conventional z-filtered TOCSY experiment,[35] RF phase coherence is required in the modified experiment to ensure that both magnetization components are kept orthogonal to the mixing sequence;[26] this is to avoid undesirable relaxation effects. A WALTZ-16[32] sequence was used for the isotropic mixing, with an 8 kHz field strength. When the two data sets are added together, the magnetization that was in the transverse plane at the beginning and the end of the mixing sequence is selected. The resulting phase-sensitive 2D spectrum is shown in Fig. 1. When the two data sets are subtracted, the magnetization that was longitudinal at the beginning and end of the mixing period is selected. The resulting spectrum is shown in Fig. 2 with exactly the same plotting parameters as for Fig. 1; this data set was processed identically to that in [illegible]. 1 except for a 90° phase shift in each dimension. Clearly the two data sets are virtually indistinguishable on this scale.

To demonstrate the improvement in sensitivity that results from adding the M_x (Fig. 1) and M_z (Fig. 2) spectra together, slices are shown in Fig. 3 that were taken parallel to the ω_1 axis through selected resonances in the three data sets M_x, M_z and $M_x + M_z$. Also included in Fig. 3 are the relevant slices taken from a spectrum obtained by combining the M_x and M_z data as quadrature pairs and performing a complex Fourier transformation in the ω_1 dimension; in this case only half of the experimental data was used, since every other FID recorded in the TPPI scheme is not required for the hypercomplex method. The data are plotted such that the r.m.s. noise level is the same for the corresponding slices from each data set; this required scaling down of the $M_x + M_z$ data by a factor of $\sqrt{2}$ relative to the other data sets. The factor of $\sqrt{2}$ is both that predicted theoretically above and

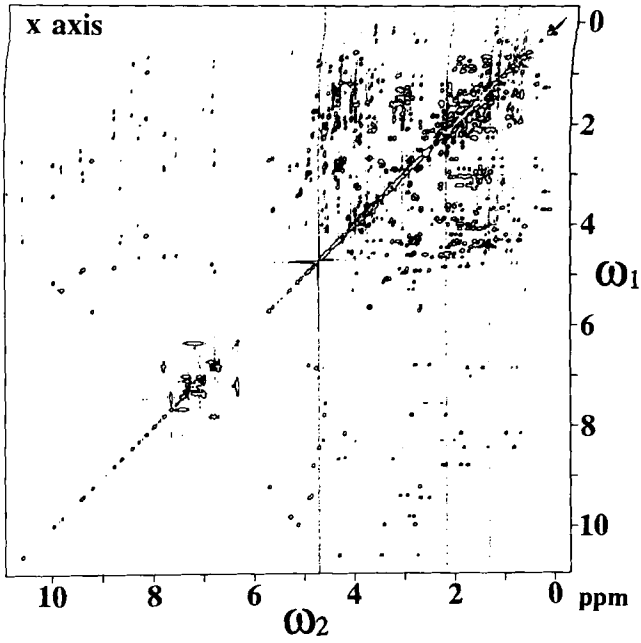

Fig. 1. Contour plot of a 2D phase-sensitive TOCSY spectrum for the protein BPTI (1 mM, in D_2O, pD 4.7, 303 K) recorded at 500 MHz (Bruker AM500) using the sensitivity-improved pulse sequence described in the text. The data shown arise from the magnetization that is aligned along the x axis of the rotating frame at the beginning and end of the mixing period (WALTZ-16 sequence has phases $+/-y$); the spectrum was generated by adding together the two data sets acquired. The WALTZ-16 sequence was applied for 69 ms, with an RF field strength of 8 kHz. The ω_2 spectral width was 12 500 Hz, 4096 data points were acquired (alternately in time) in each channel of the quadrature receiver, and 16 scans were signal-averaged for each of the two experiments needed to generate the spectrum shown. The ω_1 spectral width was 7143 Hz, and 640 t_1 values were used. A sine-bell window function, shifted by 60°, was applied in the ω_2 dimension and shifted by 45° in the ω_1 dimension. Only the positive contour levels are plotted. All data were processed using software provided by Hare Research. Suppression of t_1 ridges was accomplished by the method of Otting *et al.*[36]

that measured experimentally via numerical evaluation of the r.m.s. noise in ω_1 slices from the spectra. It can be seen in each example shown in Fig. 3 that the combined data have an improved signal-to-noise ratio compared with either the M_x or M_z data; quantitatively, the improvement in all cases is approximately $\sqrt{2}$, in agreement with theory. It is also apparent that the data treated as hypercomplex have the same signal-to-noise ratio as the M_x and M_z spectra, even though they were accumulated in half the time.

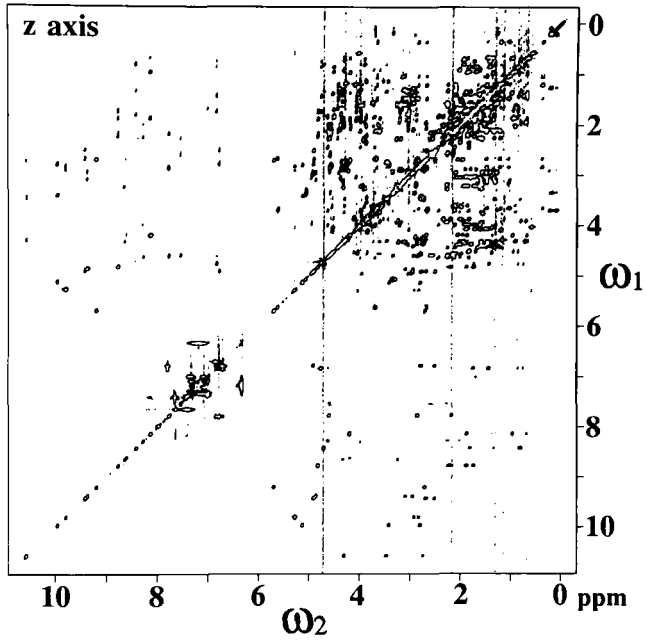

Fig. 2. Contour plot of a 2D TOCSY spectrum of BPTI, obtained from the same two data sets used to generate the spectrum in Fig. 1, except that the two sets were subtracted instead of added. The data shown arise from the magnetization that is aligned along the *z* axis of the rotating frame at the beginning and end of the mixing period. Processing parameters identical to those for the spectrum in Fig. 1 have been used, except that an additional 90° zeroth-order phase correction has been applied in both frequency dimensions.

3.2.1. Mixing sequences

The improvement in sensitivity of the TOCSY experiment as described here is based on the PEP methodology. In addition to the fact that the noise functions in the two orthogonally detected signals are uncorrelated, the sensitivity enhancement also requires that the two orthogonal magnetization components give rise to nearly identical spectra. In principle, this latter requirement would mean that the experimental mixing sequence should produce an effective Hamiltonian that retains only the isotropic scalar coupling terms. While the WALTZ-16 sequence does not produce a strictly isotropic mixing Hamiltonian,[38] the deviations are small enough to cause minimal problems. The so-called "17th pulse" proposed by Bax[26,39] to minimize the small loss in intensity due to intermixing of the orthogonal magnetization components during the mixing period is not compatible with the scheme described here for retaining two coherence transfer pathways. Mixing schemes based on the MLEV-16 sequence[26] are not useful for the sensitivity-improved TOCSY method because of non-isotropic behaviour

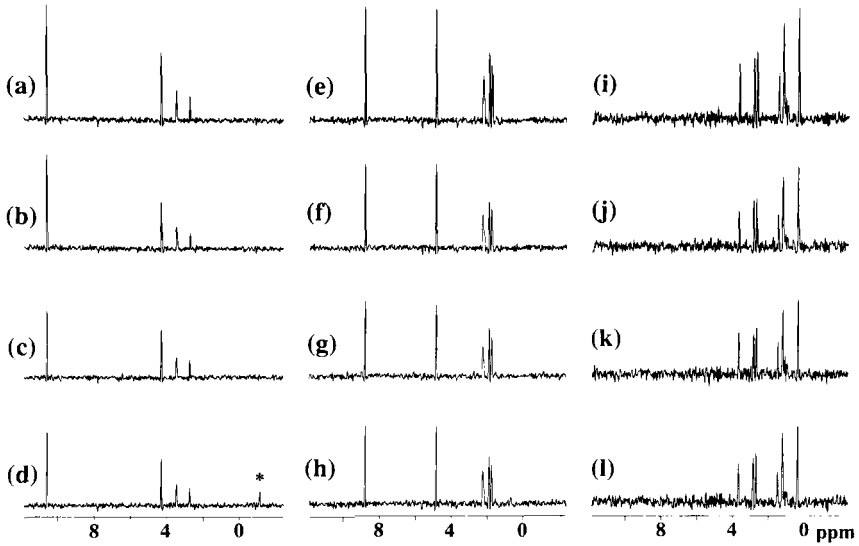

Fig. 3. Slices taken parallel to the ω_1 axis through 2D TOCSY spectra of BPTI. Slices (a)–(d) were taken at the ω_2 frequency (10.55 ppm) of the NH of tyrosine-23, slices (e)–(h) at the ω_2 frequency (8.77 ppm) of the NH of glutamine-31, and slices (i)–(l) at the ω_2 frequency (0.39 ppm) of one of the $C^{\beta}H$ of arginine-42.[37] The top row of data, slices (a), (e) and (i), was taken from the sensitivity-improved TOCSY spectrum obtained by adding together the M_x spectrum (Fig. 1) and the M_z spectrum (Fig. 2). The second row of data, slices (b), (f) and (j), was taken from the M_z spectrum, and the third row, slices (c), (g) and (k), was taken from the M_x spectrum. The bottom row of data, slices (d), (h) and (l), was taken from a data set generated by combining half of the M_x and M_z data as complex pairs before the ω_1 Fourier transformation (see text). The asterisk in slice (d) indicates an ω_1 "quadrature image" peak. Clearly the top row ($M_x + M_z$) has improved sensitivity over the M_x and M_z data, and the bottom row (complex combination) has equal sensitivity to the M_x and M_z spectra, even though the data were essentially acquired in half the time (i.e. only half the M_x and M_z data were used).

and unwanted relaxation effects. The DIPSI sequences reported by Shaka *et al.*[33] are very effective in the sensitivity-improved TOCSY experiment, since they were specifically designed to produce an isotropic mixing Hamiltonian. The DIPSI-2 and DIPSI-3 sequences are used in this context in our laboratory. One would predict that the FLOPSY sequences,[40] also introduced by Shaka, may not be applicable, for those reasons noted.

4. SENSITIVITY IMPROVEMENT IN ONE-BOND HETERONUCLEAR CORRELATION EXPERIMENTS

At present, information about the structure of proteins is mostly derived from proton NMR spectroscopy; bond connectivities are characterized by

the use of two-dimensional COSY[41,42] and TOCSY[25] experiments and interproton distances are determined by the use of two-dimensional NOESY[24] experiments. Although this approach has been fruitful for small proteins, the study of larger proteins by two-dimensional homonuclear NMR methods is limited in part by increased resonance overlap in the spectra.

One method that has been very useful in alleviating much of the resonance congestion is two-dimensional heteronuclear correlation spectroscopy.[43–45] Many assignment problems can be simplified by employing one-bond heteronuclear correlation methods, taking advantage of the larger chemical-shift dispersion of ^{13}C and ^{15}N heteronuclei. In addition to its inherent usefulness, the one-bond heteronuclear correlation experiment is also the basis for powerful heteronuclear relay experiments[46–50] and for heteronuclear relaxation measurements.[51–53] To obtain optimum sensitivity in these types of experiments, excitation and detection of proton magnetization is required.

Even with the introduction of proton-detected methods, sensitivity enhancement is always a prime concern in these types of experiments and maximizing the inherent sensitivity of the method, as in the case of the TOCSY experiment, is of paramount importance. In this section, the potential for an increase in sensitivity via PEP technology in various heteronuclear correlation methods is demonstrated. The size of the sensitivity enhancement can be as large as $\sqrt{2}$.

The principle behind the sensitivity increase for heteronuclear correlation experiments[22] is exactly the same as that described for the TOCSY experiment, by using the PEP methodology. However, modifications of the conventional sequences are required to obtain the enhancement, unlike in the TOCSY example, where only the phase cycling played a crucial part. Again, two orthogonal magnetization components are required to be detected, and it is in preserving these two components that the pulse sequences themselves need to be extended.

In Sections 4.1–4.3 methods are described for improving the sensitivity of each of the main classes of one-bond heteronuclear correlation experiments for heteronuclei with single geminal protons. An analysis of relaxation effects is presented along with experimental demonstration of the proposed methods.

4.1. Theory

The different classes of proton-detected one-bond heteronuclear correlation methods are conveniently categorized according to the form of the density operator after the initial excitation sequence and before the t_1 period. The methods can be classified as follows:

(i) sequences in which the density operator contains both I and S components that are unmodulated by chemical-shift evolution;

(ii) sequences in which the operator contains both I and S components that are encoded with the I-spin chemical shift;

(iii) sequences in which the operator contains only S-spin components.

The labels I and S refer to protons and heteronuclei respectively. The analysis below will consider the mosts popular methods belonging to each class, which are as follows:

class 1—the heteronuclear single-quantum coherence (HSQC) experiment;[44,54]

class 2—the heteronuclear multiple quantum coherence (HMQC) experiment;[44,55,56]

class 3—the double DEPT[44] and double refocused INEPT[44] experiments.

Although in the strictest definition, those experiments noted under class 3 involve the evolution of heteronuclear single quantum coherence during t_1; here they are differentiated from "conventional" HSQC experiments (class 1) by virtue of the fact that at the beginning of t_1 in-phase coherence evolves rather than antiphase coherence. (In practice, both class 1 and class 3 experiments would be referred to as HSQC methods.)

The PEP principle upon which the sensitivity-enhanced sequences are based is, of course, broadly applicable; however, the manner in which a given sequence must be modified depends on the particular nature of the experiment. Figure 4 shows the conventional pulse sequences for the HSQC, HMQC and double DEPT experiments, while Fig. 5 shows the sensitivity-enhanced versions of each of these methods. In the analysis below the spin system consists of a heteronucleus, denoted the S spin, that has one or more directly attached protons and any number of remotely connected protons, denoted the I spins. All spins are assumed to be weakly coupled, and the one-bond heteronuclear coupling between the I and S spins is assumed to be much larger than the homonuclear scalar couplings between the attached and remote I spins. In the following treatment only the product operator terms that illustrate the principles of the methods are given; other terms potentially giving rise to observable signal are experimentally suppressed by appropriate phase cycling, homospoil gradients or purge pulses.

As a fully worked example of PEP sensitivity enhancement technology in heteronuclear correlation experiments, the HSQC experiment is chosen because of its popularity in the study of proteins.[57,58] The conventional sequence (Fig. 4a) consists of an INEPT polarization transfer from the I to the S spins, a t_1 evolution period, a reverse INEPT polarization transfer

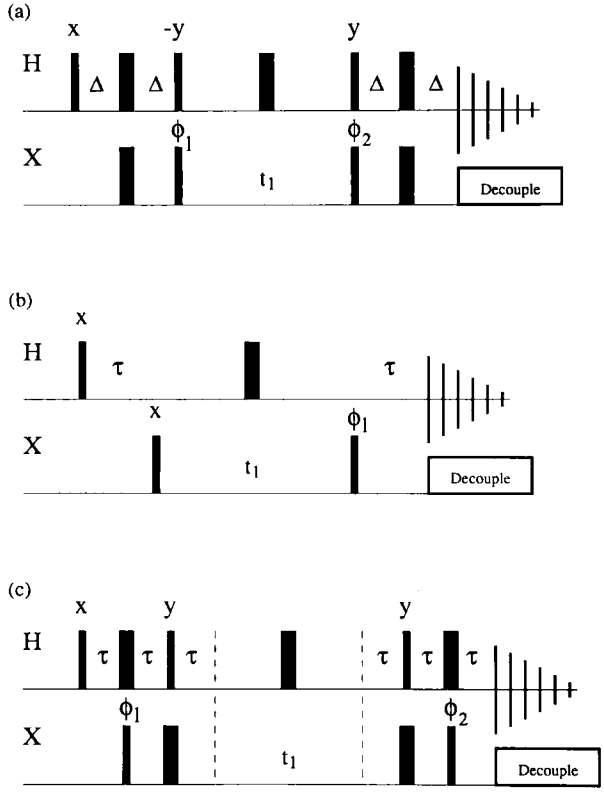

Fig. 4. Pulse sequences for recording conventional heteronuclear correlation spectra. The pulse sequences shown are for (a) the HSQC, (b) the HMQC and (c) the double DEPT methods of acquiring two-dimensional heteronuclear correlation spectra. The thin and thick vertical bars represent 90° and 180° pulses applied to the H (protons) or X (heteronucleus) spins; all 180° pulses in the sequences are applied along the y axis. The delays Δ and τ are $1/4J$ and $1/2J$ respectively, where J is the one-bond HX coupling constant. Decoupling of the X spins during acquisition is achieved by using an appropriate composite pulse decoupling sequence. Quadrature detection in the ω_1 dimension can be achieved by either the TPPI or hypercomplex methods (see text). The basic phase cycling is (a) $\phi_1 = (x, -x, x, -x)$, $\phi_2 = (x, x, -x, -x)$ and receiver = $(x, -x, -x, x)$; (b) $\phi_1 = (x, -x, -x, x)$ and receiver = $(x, -x, -x, x)$; (c) same as (a). In practice, composite 180° pulses may be used in place of the regular 180° pulses on the X spins. Heteronuclear zero- and double-quantum artefacts can be reduced by phase cycling of the 180° proton pulse in the middle of t_1.

from S to I spins, and a t_2 acquisition period. Beginning with equilibrium I-spin magnetization, the evolution up to the t_1 period is (see Figs 4a and 5a):

$$I_z \xrightarrow{\text{INEPT}} -2I_zS_y \tag{33}$$

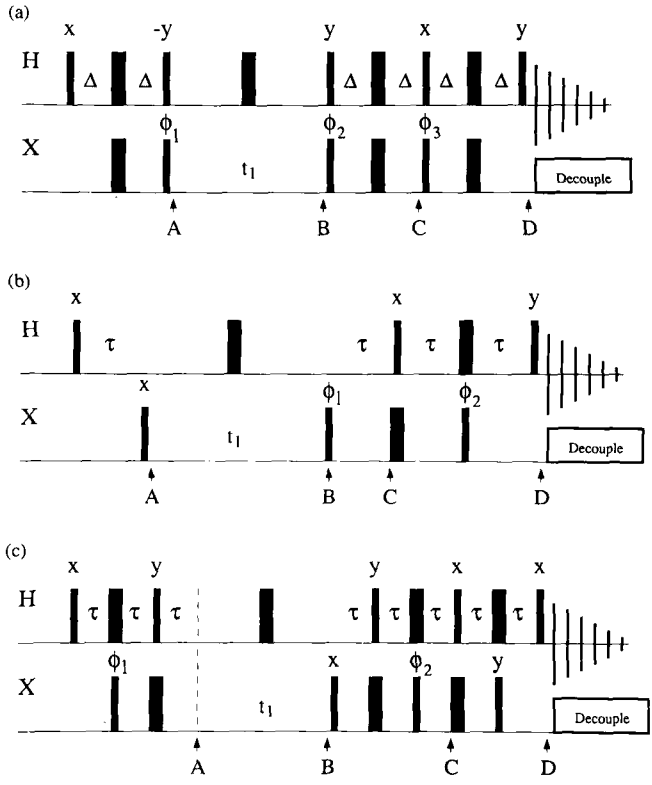

Fig. 5. Pulse sequences for recording heteronuclear correlation spectra with improved sensitivity. The pulse sequences shown are for improving the sensitivity of (a) the HSQC, (b) the HMQC and (c) the double DEPT methods of acquiring two-dimensional heteronuclear correlation spectra. The relevant product operators present at the points labelled A–D in the sequences are given in Table 1. The thin and thick vertical bars represent 90° and 180° pulses applied to the H (protons) or X (heteronucleus) spins; all 180° pulses in the sequences are applied along the y axis. The delays Δ and τ are $1/4J$ and $1/2J$ respectively, where J is the one-bond HX coupling constant. Decoupling of the X spins during acquisition is achieved by using an appropriate composite pulse decoupling sequence. Quadrature detection in the ω_1 dimension can be achieved by either the TPPI or hypercomplex methods (see text). The basic phase cycling is (a) $\phi_1 = (x, -x, x, -x)$, $\phi_2 = (x, x, -x, -x)$, $\phi_3 = (y, y, -y, -y)$ and receiver = $(x, -x, -x, x)$; (b) $\phi_1 = (x, -x, -x, x)$, $\phi_2 = (y, -y, y, -y)$ and receiver = $(x, -x, -x, x)$; (c) $\phi_1 = (x, -x, x, -x)$, $\phi_2 = (x, x, -x, -x)$ and receiver = $(x, -x, -x, x)$. In practice, composite 180° pulses may be used in place of the regular 180° pulses on the X spins. Heteronuclear zero- and double-quantum artefacts can be reduced by phase cycling of the 180° proton pulse in the middle of t_1. For sensitivity improvement, two experiments are recorded, the first with the phase cycle as noted above, the second with phase inversion of the pulse on the X spins immediately following the t_1 period. The two data sets are stored separately and then combined as described in the text.

where the delay Δ in the INEPT sequence is $1/4J_{IS}$, and J_{IS} is the one-bond heteronuclear scalar coupling constant (a factor of $\sin \pi J_{IS}\Delta$ has been dropped from (33) for convenience). During the t_1 period the antiphase operator evolves solely under the influence of the heteronuclear chemical shift because the 180° pulse on the I spins in the middle of t_1 decouples the I and S spins:

$$-2I_zS_y \xrightarrow{t_1/2-180°(I)-t_1/2} 2I_zS_y \cos \omega_S t_1 - 2I_zS_x \sin \omega_S t_1, \tag{34}$$

in which ω_S is the Larmor frequency of the decoupled S spins in the rotating reference frame. If the heteronucleus has a single attached proton, the reverse INEPT sequence gives (again dropping $\sin \pi J_{IS}\Delta$ factors),

$$2I_zS_y \cos \omega_S t_1 - 2I_zS_x \sin \omega_S t_1 \xrightarrow{\text{reverse INEPT}} I_y \cos \omega_S t_1 - 2I_xS_x \sin \omega_S t_1. \tag{35}$$

If the heteronucleus has more than one attached proton, evolution of the multiple quantum coherence term $2I_xS_x$ under heteronuclear scalar couplings to the passive spins I' occurs during the reverse INEPT sequence. In the case of two attached protons the reverse INEPT sequence would generate

$$2I_zS_y \cos \omega_S t_1 - 2I_zS_x \cos \omega_S t_1 \xrightarrow{\text{reverse INEPT}} I_y \cos \omega_S t_1 - 4I_xI'_zS_y \sin \omega_S t_1. \tag{36}$$

In (35) and (36), the $I_y \cos \omega_S t_1$ term represents I-spin magnetization that is labelled by the chemical shift of the heteronucleus during t_1 and is detected during t_2. The other terms represent multiple quantum coherences that are unobservable during t_2. For these types of experiments, where only one in-phase magnetization component is observed, the resulting two-dimensional data set can be processed into a single-bond heteronuclear correlation spectrum with peak shapes that are purely absorptive in both dimensions as expected. This is the case for the purely conventional HSQC experiment of Fig. 4(a).

The evolution of the density operator for the enhanced HSQC sequence (Fig. 5a) proceeds exactly as for the conventional HSQC experiment up to the point labelled C in Fig. 5(a), where the operators are given by the final terms in (35) and (36). For a heteronucleus with a single attached proton, (35), the evolution through the remainder of the sequence is

$$\begin{aligned} I_y \cos \omega_S t_1 - 2I_xS_x \sin \omega_S t_1 &\xrightarrow{90°_x(I)\,90°_y(S)} I_z \cos \omega_S t_1 - 2I_xS_z \sin \omega_S t_1 \\ &\xrightarrow{\Delta-180°_y(I,S)-\Delta} -I_z \cos \omega_S t_1 + I_y \sin \omega_S t_1 \\ &\xrightarrow{90°_y(I)} -I_x \cos \omega_S t_1 + I_y \sin \omega_S t_1. \end{aligned} \tag{37}$$

The resultant $-I_x \cos \omega_S t_1$ and $I_y \sin \omega_S t_1$ terms in (37) describe orthogonal

in-phase I-spin magnetization components that have evolved at the frequency of the S-spin during t_1. This state of affairs can be recognized as the basis for the sensitivity enhancement procedure, where two orthogonal in-phase magnetization components are detected simultaneously. It is also important to consider the fate of the heteronucleus with two attached protons, (36), during the final stage of the enhanced sequence:

$$\begin{aligned} I_y \cos\omega_S t_1 - 4I_x I_z' S_y \sin\omega_S t_1 &\xrightarrow{90^\circ_x(I)\,90^\circ_y(S)} I_z \cos\omega_S t_1 + 4I_x I_y' S_y \sin\omega_S t_1 \\ &\xrightarrow{\Delta\text{–}180^\circ_y(I,S)\text{–}\Delta} -I_z \cos\omega_S t_1 - 4I_x I_y' S_y \sin\omega_S t_1 \\ &\xrightarrow{90^\circ_y(I)} -I_x \cos\omega_S t_1 + 4I_z I_y' S_y \sin\omega_S t_1. \end{aligned} \quad (38)$$

The first term in the final expression of (38) represents in-phase I-spin magnetization, while the second term represents unobservable multiple quantum coherence. In this case, for a heteronucleus with two attached protons, the modified sequence does not generate the required two orthogonal components for sensitivity improvement; consequently, the extended sequences do not provide sensitivity enhancement for heteronuclei with two geminal protons. Similar conclusions hold for heteronuclei with more than two attached protons.

The resulting two terms in (37) give rise to the observable signals, which are 90° out of phase in both dimensions; processing of these data alone would generate a phase-twisted spectrum. As outlined in the basic PEP methodology, it is necessary to separate the two orthogonal terms and obtain purely absorptive spectra by recording a second experiment in which one of the detected terms in (37) changes sign. This is easily achieved by executing the extended sequence again, but with inversion of the phase of the 90° pulse on the heteronucleus immediately following the t_1 period. In this experiment the relevant operator terms are (beginning with the operators at the end of (34)),

$$2I_z S_y \cos\omega_S t_1 - 2I_z S_x \sin\omega_S t_1$$

$$\xrightarrow{90^\circ_y(I)\,90^\circ_{-x}(S)\text{–}\Delta\text{–}180^\circ_y(I,S)\text{–}\Delta\text{–}90^\circ_x(I)\,90^\circ_y(S)\text{–}\Delta\text{–}180^\circ_y(I,S)\text{–}\Delta\text{–}90^\circ_y(I)}$$

$$I_x \cos\omega_S t_1 + I_y \sin\omega_S t_1, \quad (39)$$

for a single attached proton. For a heteronucleus with two attached protons the second experiment yields

$$2I_z S_y \cos\omega_S t_1 - 2I_z S_x \sin\omega_S t_1$$

$$\xrightarrow{90^\circ_y(I)\,90^\circ_{-x}(S)\text{–}\Delta\text{–}180^\circ_y(I,S)\text{–}\Delta\text{–}90^\circ_x(I)\,90^\circ_y(S)\text{–}\Delta\text{–}180^\circ_y(I,S)\text{–}\Delta\text{–}90^\circ_y(I)}$$

$$I_x \cos\omega_S t_1 + 4I_z I_y' S_y \sin\omega_S t_1. \quad (40)$$

Following the above analysis, it is now possible to write general expressions to describe the observable operators at the beginning of the acquisition period for the modified experiment. For the first experiment the observable operators are

$$-I_x \cos \omega_S t_1 + \delta_{1n} I_y \sin \omega_S t_1, \tag{41}$$

and for the second experiment

$$I_x \cos \omega_S t_1 + \delta_{1n} I_y \sin \omega_S t_1 \tag{42}$$

in which δ_{1n} is the Kronecker delta and n is the number of protons directly attached to the heteronucleus. Addition of the two data sets (41) and (42) yields the single observable term

$$2\delta_{1n} I_y \sin \omega_S t_1, \tag{43}$$

while subtraction gives the single observable term

$$-2I_x \cos \omega_S t_1. \tag{44}$$

Neglecting relaxation effects and pulse imperfections in the longer sequences, the spectrum that results from the $-2I_x \cos \omega_S t_1$ term is identical to the spectrum obtained using the conventional HSQC sequence. When one neglects relaxation, mismatching between the one-bond heteronuclear coupling constants and the delay Δ, and pulse imperfections, the spectrum that results from the $2\delta_{1n} I_y \sin \omega_S t_1$ term produces a two-dimensional heteronuclear correlation spectrum that has been edited with a multiplicity filter.[55,59] In this spectrum the resonances that arise from heteronuclei with one attached proton have the same intensities as those in the conventional spectrum, but the resonances of other heteronuclei are nulled. These two spectra are obtained using the enhanced sequence of Fig. 5(a) in the same amount of time required to obtain one spectrum using the conventional HSQC sequence of Fig. 4(a).

The final sensitivity-enhanced spectrum is obtained by adding the two pure absorption spectra derived above. As described earlier for the PEP technique, the resultant spectrum has resonances that are coherent combinations of the two separate spectra, whereas the r.m.s. noise in this process combines as though statistically independent and increases only by $\sqrt{2}$. Neglecting relaxation effects, the theoretical increase in signal-to-noise ratio of the enhanced experiment over the conventional one is $\sqrt{2}$. For convenience in the discussion above the equivalent data sets were presumed to have been processed separately and then co-added as 2D spectra. As pointed out in Section 2.3.1, it is also possible to combine the data in the time-domain using the appropriate recipe if the hypercomplex method for ω_1 sign discrimination has been employed.

The other sensitivity-enhanced sequences shown in Fig. 5 work in virtually the same way as described for the HSQC sequence. First, the operator that

Table 1. Product operators for pulse sequences with enhanced sensitivity.[a]

Point	HSQC
A	$-2I_zS_y$
B	$2I_zS_y\cos\omega_S t_1 - 2I_zS_x\sin\omega_S t_1$
C	$I_y\cos\omega_S t_1 - 2I_xS_x\sin\omega_S t_1$
D	$-I_x\cos\omega_S t_1 + I_y\sin\omega_S t_1$
Point	**HMQC**
A	$-2I_xS_y\cos\omega_I\tau - 2I_yS_y\sin\omega_I\tau$
B	$2(I_x\cos\omega_I\tau - I_y\sin\omega_I\tau)(S_y\cos\omega_S t_1 - S_x\sin\omega_S t_1)$
C	$I_y\cos\omega_S t_1 - 2I_x\sin\omega_S t_1(S_x\cos\omega_S\tau + S_y\sin\omega_S\tau)$
D	$-I_x\cos\omega_S t_1 + I_y\sin\omega_S t_1$
Point	**Double DEPT**
A	S_x
B	$S_x\cos\omega_S t_1 + S_y\sin\omega_S t_1$
C	$-I_y\cos\omega_S t_1 - 2I_z\sin\omega_S t_1(S_x\cos\omega_S\tau + S_y\sin\omega_S\tau)$
D	$-I_y\cos\omega_S t_1 - I_x\sin\omega_S t_1$

[a]The table shows the principal product operators, for a heteronuclear S spin with a single geminal proton I spin, that are present at the points labelled A–D in Fig. 5 for the sensitivity-enhanced HSQC, HMQC and double DEPT pulse sequences. The terms at point D are detected during the acquisition period; the sign of one of the components can be negated by inverting the phase of the first 90° pulse on the S spins following the t_1 period in Fig. 5. The operators at point A and B are identical to the operators at the corresponding points in the conventional sequences shown in Fig. 4. The operators at point C are identical to the operators prior to acquisition in the conventional HSQC and HMQC sequences; for the conventional double DEPT sequence the operator terms are: $-I_y\cos\omega_S t_1 - 2I_x\sin\omega_S t_1(S_X\cos\omega_S\tau + S_y\sin\omega_S\tau)$.

is cosine-modulated during t_1 is transferred to a single-quantum I-spin operator. Secondly, this operator is stored as longitudinal magnetization while the product operator that is sine-modulated during t_1 is refocused to transverse proton magnetization. Thirdly, the final proton 90° pulse rotates the longitudinal magnetization back to the transverse plane for detection. In all cases a second experiment is acquired in which the phase of the first 90° pulse on the heteronuclei after t_1 is inverted and the data are processed as described. The product operators present at the most informative points in each of the sequences in Fig. 5 are given in Table 1.

Unlike in the enhanced TOCSY experiment, the sensitivity-enhanced heteronuclear correlation sequences have been extended in duration. Consequently the maximum signal-to-noise enhancement of $\sqrt{2}$ is only achievable if relaxation of the density operator during the pulse sequences is negligible. In general, owing to additional relaxation processes during the longer pulse sequences, the magnitudes of the two orthogonal I-spin

operators that are acquired in the enhanced experiments will be less than the magnitudes of the I-spin operators present during the acquisition period in the conventional experiments. In addition, the magnitudes of the two orthogonal magnetization components in the enhanced sequences will not be equal, because the cosine- and sine-modulated operators present after the t_1 period follow different pathways during the reverse polarization transfer steps and relax at different rates. For these reasons, the sensitivity gains afforded by the methods described here will be reduced from the ideal value of $\sqrt{2}$ by amounts that depend on both the relative lengths of the conventional and enhanced pulse sequences and the particular product operator terms present during the polarization transfer from the heteronucleus back to proton.

4.2. Relaxation considerations

Once again, for illustrative purposes, the conventional and enhanced HSQC sequences are considered.[22] During the reverse INEPT transfer in the conventional experiment, the heteronuclear antiphase operator I_xS_z is refocused to I_y. The magnitude of the observable operator at the beginning of the t_2 acquisition period is, disregarding the chemical shift modulation,

$$I_y = I_y^0 \exp(-2R_{2I}\Delta), \tag{45}$$

in which R_{2I} is the average of the transverse relaxation rate constants of the in-phase and antiphase I-spin operators, and I_y^0 is the magnitude of the operator in the absence of relaxation.

In the enhanced experiment two consecutive reverse INEPT sequences, each of length 2Δ, are used to refocus the heteronuclear operators present after t_1 into orthogonal I_x and I_y operators. The magnitude of each of the I_x and I_y operators depends on the relaxation of the operators present during each of the reverse INEPT sequences. Inherent within the reverse INEPT portion of (35), a cosine-modulated I_xS_z term is refocused to an I_y term during the first INEPT transfer. The second INEPT sequence then simply stores this term as longitudinal magnetization, and it is finally converted to the I_x operator by the last 90° pulse for detection. In the second INEPT sequence the initial I_z operator relaxes toward the thermal equilibrium polarization during the first delay Δ; then the 180° pulse on the I spins inverts the I_z term to $-I_z$, which proceeds to relax towards thermal equilibrium during the second Δ delay. The operator prior to the final pulse of the sequence is

$$I_z = I_z^\infty - [2I_z^\infty - (I_z^\infty - I_z^0)\exp(-R_{1I}\Delta)]\exp(-R_{1I}\Delta), \tag{46}$$

in which I_z^∞ is the thermal-equilibrium value of the longitudinal magnetization, I_z^0 is the value of the longitudinal magnetization at the beginning of the

second reverse INEPT sequence, and R_{1I} is the longitudinal relaxation rate constant for the I spins. Because of the phase cycling of the 90° pulses on the S spins and of the receiver (Fig. 5a), the value of I_z^0 is inverted on alternate scans and the resulting signals are subtracted. The average relaxation of I_z over the phase cycle is found by changing the sign of I_z^0 in (46) and subtracting the new result from (46) to yield

$$I_z = -I_z^0 \exp(-2R_{1I}\Delta). \tag{47}$$

During the 2Δ period, cross-relaxation can also occur between I spins, which would be expected to produce NOESY peaks in the spectrum described by the term $-2I_x \cos \omega_S t_1$; however, since Δ is short, such peaks are expected to be extremely weak and very difficult to observe. Using (45) and (47), it is now possible to calculate the magnitude of the final observable cosine-modulated I_x operator, disregarding chemical-shift modulation,

$$I_x = I_x^0 \exp[-2(R_{2I} + R_{1I})\Delta], \tag{48}$$

in which I_x^0 is the magnitude of the operator in the absence of relaxation. The sine-modulated component, I_y, following t_1, is stored as I_xS_x multiple quantum coherence during the first reverse INEPT sequence (35) and refocused from I_xS_z to I_y during the second reverse INEPT transfer (37). The magnitude of the final observable operator is, disregarding chemical-shift modulation,

$$I_y = I_y^0 \exp[-2(R_{2I} + R_{2MQ})\Delta], \tag{49}$$

in which R_{2MQ} is the average of the transverse relaxation rates of the zero and double-quantum coherences present during the first INEPT sequence, and I_y^0 is the magnitude of the operator in the absence of relaxation.

The relative intensities of the conventional HSQC spectrum and the spectra that result from addition, (43), and subtraction, (44), of the two data sets acquired with the enhanced sequence can be determined from (45), (48) and (49). The relative intensities of the spectra that result from addition and subtraction compared with the conventional sequence are

$$E_{add} = \exp(-2R_{2MQ}\Delta), \tag{50}$$

$$E_{sub} = \exp(-2R_{1I}\Delta) \tag{51}$$

respectively. The relative intensity of the added spectrum compared with the subtracted spectrum is

$$E_r = \frac{E_{add}}{E_{sub}}, \tag{52}$$

Table 2. Effects of relaxation in pulse sequences with enhanced sensitivity.[a]

	ε_a	ε_s
HSQC	$\exp(-2R_{2MQ}\Delta)$	$\exp(-2R_{1I}\Delta)$
HMQC	$\exp(-2R_{2MQ}\tau)$	$\exp(-2R_{1I}\tau)$
DEPT	$\exp(-2R_{1S}\tau)$	$\exp(-2R_{1I}\tau)$

[a]The table shows the relative intensities of the two spectra obtained by deconvoluting the two orthogonal in-phase magnetization components that are obtained in the sensitivity-enhanced heteronuclear correlation experiments (Fig. 5), compared with the corresponding conventional spectra (Fig. 4). The relative intensities ε_a and ε_s refer to the ADD and SUBTRACT spectra respectively. The notation is described in the text.

where $E_r < 1$ since R_{2MQ} will generally be greater than R_{1I}. The achievable sensitivity enhancement is

$$E = \tfrac{1}{2}\sqrt{2}(E_{add} + E_{sub}), \tag{53}$$

compared with the maximum value of $\sqrt{2}$. The analysis of the effects of relaxation of the other sensitivity-enhanced pulse sequences follow similar lines. The results for the relative intensities of the two independent deconvoluted data sets are given in Table 2.

To estimate the expected sensitivity enhancement for a given molecule, the appropriate relaxation rates, given in (50) and (51) and Table 2, must be measured experimentally or calculated for a specific relaxation mechanism. In the following the I and S spins are assumed to relax solely by dipole–dipole interactions, and the spins are assumed to be rigidly attached to a molecule that undergoes isotropic rotational diffusion with a correlation time τ_c. The S spins relax only through interactions with the directly attached I spins; the I spins relax both with the S spins and with other nearby I spins. Other relaxation mechanisms are not considered. The I spins are assumed to be in the slow-motion limit with $\omega_I\tau_c \gg 1$ and $\omega_I \gg \omega_S$, where ω_I and ω_S are the Larmor frequencies of the I and S spins respectively.

The expressions for the dipolar relaxation rate constants for the longitudinal I_z and S_z operators and for the transverse multiple quantum operator are given by

$$R_{1I} = \frac{1}{10} D_{IS}^2[J(\omega_I - \omega_S) + 3J(\omega_I) + 6J(\omega_I + \omega_S)] + \frac{1}{10}\sum_k D_{IK}^2[J(0) + 3J(\omega_I) + 6J(2\omega_I)], \tag{54}$$

$$R_{1S} = \frac{1}{10} D_{IS}^2[J(\omega_I - \omega_S) + 3J(\omega_I) + 6J(\omega_I + \omega_S)], \tag{55}$$

$$R_{2MQ} = \frac{1}{20} D_{IS}^2[J(\omega_I - \omega_S) + 3J(\omega_I) + 3J(\omega_S) + 6J(\omega_I + \omega_S)]$$

$$+ \frac{1}{20} \sum_k D_{IK}^2[5J(0) + 9J(\omega_I) + 6J(2\omega_I)], \tag{56}$$

in which

$$D_{IJ} = \frac{h\gamma(I)\gamma(J)\mu_0}{8\pi^2 r_{IJ}^3}, \tag{57}$$

$$J(\omega) = \frac{\tau_c}{1 + \omega^2\tau_c^2} \tag{58}$$

where h is Planck's constant, $\gamma(I)$ and $\gamma(J)$ are the magnetogyric ratios of the spins I and J respectively, r_{IJ} is the length of the internuclear vector between the I and J spins, and μ_0 is the permeability of free space. The summation sign includes all of the homonuclear $K \neq I$ (proton) spins. The longitudinal relaxation rate constant of the S spins, R_{1S}, is required for the analysis of the double DEPT sequence. The terms containing D_{IS} arise from the heteronuclear dipolar coupling between the I and S spins, and the terms containing D_{IK} reflect the homonuclear dipolar coupling between I spins.

In the limit of slow overall tumbling, as is the case for most biomolecules, $J(0) > J(\omega_S) \gg J(\omega_I)$; therefore the relaxation rate constants are approximately given by

$$R_{1I} = D_{IS}^2 J(\omega_I) + \frac{1}{10} J(0) \sum_k D_{IK}^2, \tag{59}$$

$$R_{iS} = \frac{3}{10} D_{IS}^2 J(\omega_S), \tag{60}$$

$$R_{2MQ} = \frac{3}{20} D_{IS}^2 J(\omega_S) + \frac{1}{4} J(0) \sum_k D_{IK}^2. \tag{61}$$

As noted elsewhere,[43,60] the expressions for the heteronuclear dipolar contribution to R_{2MQ} do not depend on $J(0)$, and hence vanish as $\tau_c \to \infty$. However, R_{2MQ} can still be large, because the magnitudes of the homonuclear dipolar terms increase monotonically with τ_c. Typically, for molecules under conditions such that $\omega_S\tau_c \gg 1$, $R_{2MQ} > R_{1I} > R_{1S}$. Keeping this inequality in mind, the results in Table 2 suggest that the attainable sensitivity enhancement would be greatest for the double DEPT, followed by the HSQC and lastly the HMQC enhanced experiments. Although this is the case theoretically, it should be noted that the enhanced double DEPT

sequence is considerably longer than the other enhanced sequences, and in practice may not have a higher absolute sensitivity.

Substituting (59) and (61) in (50) and (51) gives, for the HSQC case under consideration,

$$E_{\text{add}} = \exp\left\{-2\Delta\left[\frac{3}{20}\ D_{IS}^2 J(\omega_S) + \ \frac{1}{4} J(0)\ \sum_k D_{IK}^2\right]\right\}, \tag{62}$$

$$E_{\text{sub}} = \exp\left\{-2\Delta\left[D_{IS}^2 J(\omega_I) + \ \frac{1}{10} J(0)\ \sum_k D_{IK}^2\right]\right\}. \tag{63}$$

Similar expressions can be found for the other sequences. The expressions for E_{add} and E_{sub} for the sensitivity-enhanced sequences are dominated by the term

$$J(0) \sum_k D_{IK}^2 = \left[\frac{h\gamma(I)^2 \mu_0}{8\pi^2}\right]^2 \tau_c \sum_k r_{IK}^{-6} \tag{64}$$

for large proteins with long rotational correlation times. In the absence of significant internal motions, the largest molecules for which the longer sensitivity-enhanced HSQC sequence will yield appreciable gains in the signal-to-noise ratio of the heteronuclear correlation spectra are determined by the values of the parameters in (64). Using a typical value of $\Sigma_k r_{IK}^{-6} = 0.027\ \text{Å}^{-6} \pm 0.009\ \text{Å}^{-6}$ for the distances from a backbone proton to the other protons in proteins,[22] enhancement factors of greater than 1.1 are estimated to be obtainable for molecules with molecular correlation times of the order of 20 ns. The average value of $\Sigma_k r_{IK}^{-6}$ was calculated from the atomic coordinates of the zinc finger Xfin-31, BPTI, french bean plastocyanin and sperm whale myoglobin obtained from the Brookhaven Protein Data Bank. Distances were calculated from each backbone amide or alpha proton (except for the alpha protons of glycines) to the other protons in the protein, and the summation executed.

4.3. Experimental demonstration

In the study of proteins, sensitivity-enhanced heteronuclear correlation experiments are most useful for correlating the backbone α-carbons or amide nitrogens with their attached protons. Except for the α-carbon of glycine, the imino nitrogen of proline, and the *N*-terminal amide, these heteronuclei all have a single geminal proton, as required for sensitivity enhancement. In addition, the multiplicity-filtered spectrum that can also be obtained in these experiments assists in distinguishing backbone resonances from side-chain resonances with similar chemical shifts.

The sensitivity gains predicted theoretically were verified experimentally by the acquisition of two-dimensional heteronuclear correlation spectra using the conventional HSQC pulse sequence and the corresponding sensitivity-enhanced sequence.[22] The relevant phase cycling schemes are given in the figure captions to Figs 4 and 5. All experiments were performed on a sample of the small globular protein BPTI (MW = 6500) at ^{15}N *natural abundance*. The experimental protocol is given in the caption to Fig. 6. The total acquisition was 20 h each for the conventional HSQC experiment and the sensitivity-enhanced HSQC experiment. A contour plot of the conventional HSQC spectrum is shown in Fig. 6(a). The two data sets acquired in the sensitivity-enhanced experiment are independent combinations of two orthogonal in-phase proton magnetization components, which, if processed independently, would generate spectra with unacceptable phase-twisted lineshapes. To deconvolute the two magnetization components, the two data sets were added to produce a new data set called ADD and subtracted to produce a second data set labelled SUBTRACT. Following two-dimensional Fourier transformation and appropriate phasing, two pure absorption HSQC spectra are obtained; these spectra are shown in Fig. 6(b) for the ADD spectrum and Fig. 6(c) for the SUBTRACT spectrum. The sensitivity-enhanced spectrum is produced by adding the ADD and SUBTRACT spectra. This spectrum is shown in Fig. 6(d), and is labelled ENHANCED. For comparison purposes, cross-sections taken parallel to the ω_2 dimension from all four types of spectra are shown in Fig. 7 for selected heteronuclear resonances.

On close inspection of the two-dimensional spectra and the cross-sections it is seen that the SUBTRACT and conventional HSQC spectra are virtually identical; however, some resonances in the ADD spectrum exhibit drastically reduced intensities relative to those of both the conventional and SUBTRACT HSQC spectra. These resonances, indicated by arrows in

---

Fig. 6. Contour plots of two-dimensional ^1H–^{15}N HSQC spectra of BPTI acquired using conventional and sensitivity-enhanced HSQC methods. All experiments were performed on a sample of BPTI (20 mM, 90% H_2O/10% D_2O, pH 4.6, 308 K) at natural ^{15}N abundance. Spectroscopy was performed on a Bruker AM500 spectrometer equipped with 451 MHz IF electronics. Data processing was performed using software provided by Hare Research. A conventional HSQC spectrum was acquired using the pulse sequence of Fig. 4(a). For this experiment 1024 scans were acquired per t_1 increment. The two data sets required to produce the sensitivity-enhanced HSQC spectrum (Fig. 5a) were acquired with 512 scans per t_1 increment. For all spectra 4096 real data points (2048 per quadrature channel) were acquired in t_2 and 100 real points were acquired in t_1. TPPI was used for frequency discrimination in the ω_1 dimension. The spectral width was 7042 Hz in ω_2 and 2500 Hz in ω_1. The delay Δ was set to 2.3 ms, which is slightly less than $1/4J$ to reduce relaxation losses. To

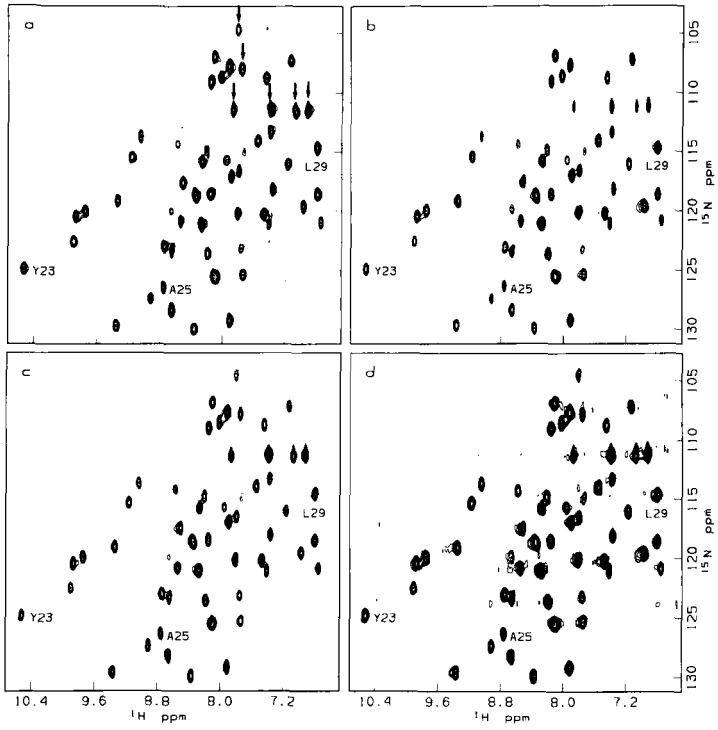

improve the suppression of magnetization from protons not bound to ^{15}N, a homospoil gradient pulse of 3 ms was applied directly after the second 90° proton pulse. The gradient pulse was followed by a delay of 7 ms to allow the magnetic field to stabilize prior to the first 90° heteronucleus pulse. The two data sets acquired using the sequence of Fig. 5(a) were added and subtracted to produce the new data sets, called respectively ADD and SUBTRACT, which were used for subsequent data manipulation. Spectra were processed using 8 Hz exponential line broadening in ω_2 and a Kaiser window in ω_1. Spectra were zero-filled before Fourier transformation to yield a final size of 2048 real points in each dimension. The spectra shown are (a) the conventional HSQC spectrum, (b) the ADD spectrum and (c) the SUBTRACT spectrum. The SUBTRACT spectrum was initially phased to be pure absorption in both dimensions; the ADD spectrum was also phased to be pure absorption in both dimensions by adding a 90° phase shift in both dimensions relative to the SUBTRACT spectrum. The ADD and SUBTRACT spectra were then added to produce the ENHANCED spectrum shown in (d). All two-dimensional spectra are shown on the same absolute scale. Arrows in (a) indicate resonances arising from the side-chain groups noted. The conventional and SUBTRACT spectra are virtually identical, while the ADD spectrum exhibits attenuated resonances in some regions (those indicated by arrows in (a)) due to the multiplicity filter. Assignments for selected resonances for comparison in Fig. 7 are also noted. For the 49 backbone amide resonances identified the ENHANCED HSQC spectrum displays a 1.32 sensitivity improvement over the conventional HSQC spectrum.

Fig. 6(a), were identified, using a conventional double-refocused INEPT experiment, as side-chain NH_2 groups (data not shown). As noted above, NH_2 resonances are suppressed in the ADD spectrum because only NH resonances are retained by the multiplicity filter in the sensitivity-enhanced sequences. In principle, these peaks should be completely absent in the ADD spectrum, but, because of mismatching of the Δ delays and the one-bond NH coupling, small residual components may remain. An example of the suppression of NH_2 resonances in the ADD spectrum is clearly demonstrated in the spectrum shown in Fig. 7(d). The ability to distinguish NH_2 side-chain groups from backbone NH groups within one experiment is a useful bonus to this methodology.

As discussed theoretically, the ideal sensitivity enhancement of $\sqrt{2}$ depends on the noise being uncorrelated in the ADD and SUBTRACT spectra, and the achievable sensitivity enhancement depends on the longitudinal and multiple quantum relaxation rates of the I and S spins. For the conventional HSQC spectrum, and the ADD, SUBTRACT and ENHANCED spectra, the magnitudes of the r.m.s. baseline noise were calculated and the intensities of 49 resolved amide peaks were determined. The levels of the r.m.s. noise in the ADD, SUBTRACT and ENHANCED spectra relative to the intensity in the conventional HSQC spectrum, the ADD spectrum and SUBTRACT spectrum were nearly identical. The ratio of the r.m.s. noise in the ENHANCED spectrum to that in the conventional HSQC spectrum was 1.35, in agreement with the expected $\sqrt{2}$. For each amide peak the values of E_{add}, E_{sub} and E were calculated as the ratios of the intensities of the resonance in the conventional HSQC spectrum respectively. A substantial sensitivity increase is realized, as seen in Fig. 7. The relative intensities and signal-to-noise enhancement are given for these selected resonances in the figure caption. The average values for all 49 resonances were $E_{add} = 0.88 \pm 0.09$, $E_{sub} = 0.99 \pm 0.07$ and $E_r = 0.89 \pm 0.08$. The average improvement in signal-to-noise ratio in the ENHANCED spectrum compared to that in the conventional HSQC spectrum was $E = 1.32 \pm 0.10$ on the basis of the theoretical increase in the r.m.s. noise.

In accordance with the described analysis of the effects of relaxation on the longer enhanced pulse sequences, the overall sensitivity enhancement obtained for the ^1H–^{15}N heteronuclear correlation spectra of BPTI was slightly less than $\sqrt{2}$. Theoretical values of $E_{add} = 0.92$, $E_{sub} = 0.97$ and $E = 1.34$ were estimated for BPTI using the details outlined above and a molecular correlation time of 4 ns.[62] The close correspondence between the empirical and calculated values suggests that pulse imperfections and evolution of homonuclear scalar couplings are not seriously detrimental to the performance of the sensitivity-enhanced method. In principle, amide proton exchange could also diminish the observed sensitivity enhancements; however, no correlation was seen between resonances having below average

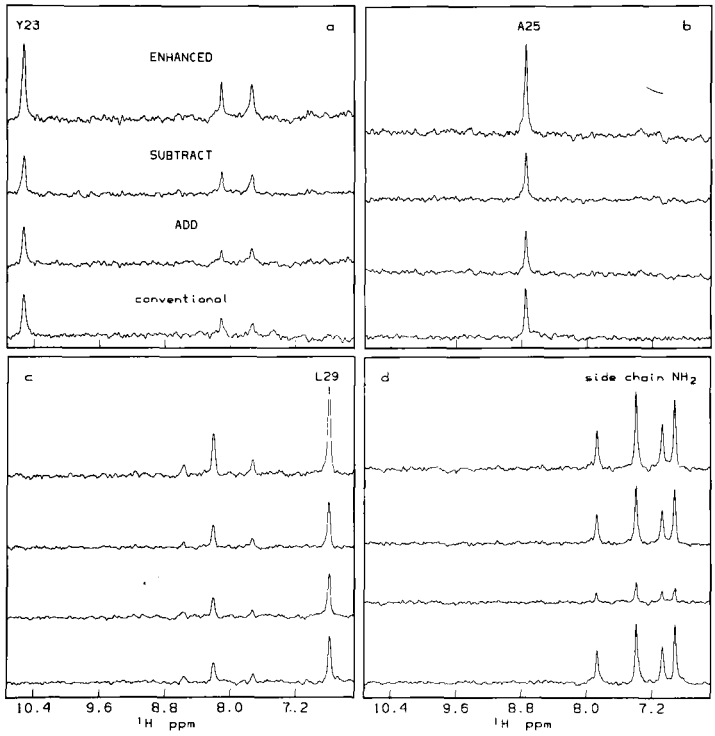

Fig. 7. Cross-sections taken parallel to the ω_2 axis, through selected N–H resonances, from the two-dimensional spectra shown in Fig. 6. Cross-sections are shown for the amide resonances of (a) Tyr 23, (b) Ala 25 and (c) Leu 29.[61] The NH_2 resonances with a ^{15}N chemical shift of 115 ppm, indicated by arrows in Fig. 6(a), are also shown. In each case the bottom trace is taken from the conventional HSQC spectrum, the second trace from the ADD spectrum, the third trace from the SUBTRACT spectrum, and the top trace from the ENHANCED spectrum. The slices are plotted on an absolute intensity scale to demonstrate clearly the noise combination characteristics. In each case the sensitivity improvement of the ENHANCED spectrum over the conventional spectrum is clear, and has been measured for the respective examples as (a) 1.26, (b) 1.31 and (c) 1.36. The slices in (d) illustrate the effect of the multiplicity filter of the ADD spectrum. In the conventional HSQC and SUBTRACT spectra four peaks are clearly visible, corresponding to two NH_2 groups, but these resonances have been suppressed in the ADD spectrum.

enhancements and amides that have been reported to undergo rapid exchange in BPTI.[63]

5. SENSITIVITY IMPROVEMENT IN PROTON-DETECTED TWO-DIMENSIONAL HETERONUCLEAR RELAY SPECTROSCOPY

Two-dimensional one-bond heteronuclear correlation NMR spectroscopy correlates a heteronucleus X with its directly connected protons H^c, as discussed above. In the proton-detected heteronuclear single-quantum coherence (HSQC)[54] version of this experiment polarization is transferred from H^c to X using an INEPT sequence,[59] allowed to evolve as heteronuclear single-quantum coherence during t_1, transferred back to H^c with a reverse INEPT sequence, and detected as proton magnetization. Two-dimensional Fourier transformation of these data generates peaks at the chemical shift of the X nucleus in the ω_1 dimension and H^c in the ω_2 dimension.

The heteronuclear NMR resonances of small biomolecules can often be assigned directly from one-bond correlation spectra if the proton resonances have been assigned previously; however, this approach alone is insufficient for larger molecules with complex proton NMR spectra. Two-dimensional heteronuclear relay spectroscopy allows the observation of correlations between a heteronucleus and protons H^r that are remotely connected, and can alleviate problems due to spectral overlap in the one-bond correlation spectra. In the proton-detected version the magnetization transfer pathway proceeds as $H^c \rightarrow X \rightarrow H^c \rightarrow H^r$, and relay peaks appear at the X nucleus chemical shift in the ω_1 dimension and the H^r chemical shift in the ω_2 dimension. Following the one-bond HSQC sequence, coherence transfer between the H^c and H^r scalar-coupled protons can be obtained by either appending a COSY-type sequence to allow the development of antiphase magnetization between the coupled protons[47,64] or, preferably, by a TOCSY-type isotropic mixing sequence.[48,49] In practice, the isotropic mixing-based heteronuclear relay experiment is by far the method of choice. The conventional pulse sequence to do this is shown in Fig. 8(a).

5.1. Theory

By simple inspection of Fig. 8(a) it is clear that the conventional heteronuclear relay pulse sequence is merely a direct combination of the two experiments described above; the one-bond HSQC experiment and the homonuclear TOCSY experiment. It is therefore not surprising that one can employ the same PEP procedures described above to increase the sensitivity of the relay method.[65]

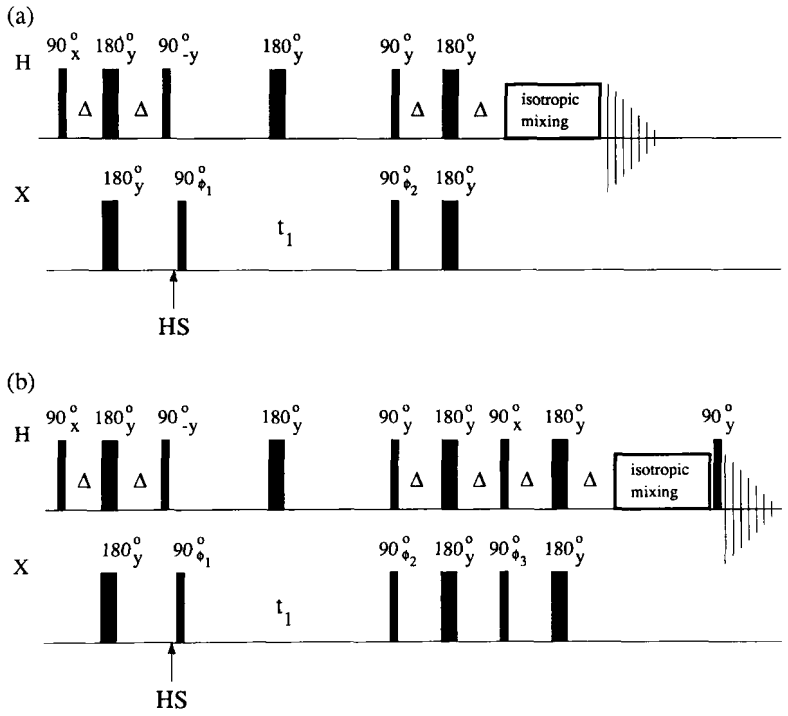

Fig. 8. Pulse sequences for heteronuclear relay correlation spectroscopy. (a) Pulse sequence to record a conventional two-dimensional ^{1}H-detected heteronuclear relay spectrum. Initially, an HSQC experiment establishes one-bond heteronuclear correlations, and then the resulting in-phase magnetization component passes into the isotropic mixing period for homonuclear coherence transfer. The phase cycling used is $\phi_1 = (x, -x, x, -x, -x, x, -x, x)$, $\phi_2 = (x, x, -x, -x)_2(-x, -x, x, x)_2$, and receiver = $(x, -x, -x, x, -x, x, x, -x, -x, x, x, -x, x, -x, -x, x)$. (b) Pulse sequence to record a sensitivity-enhanced two-dimensional ^{1}H-detected heteronuclear relay spectrum. Following the HSQC part of the sequence, two orthogonal in-phase magnetization components are refocused and both allowed to pass into the isotropic mixing scheme. Two data sets are acquired and deconvoluted to produce two pure absorption heteronuclear relay spectra that are added together to obtain a sensitivity-enhanced spectrum as described in the text. For the first data set the phase cycling is $\phi_1 = (x, -x, x, -x, -x, x, -x, x)$, $\phi_2 = (x, x, -x, -x)_2(-x, -x, x, x)_2$, $\phi_3 = (y, y, -y, -y)_2(-y, -y, y, y)_2$, and receiver = $(x, -x, -x, x, -x, x, x, -x, -x, x, x, -x, x, -x, -x, x)$; for the second data set the phase of ϕ_2 is inverted to yield $\phi_2 = (-x, -x, x, x)_2(x, x, -x, -x)_2$. In both sequences (a) and (b) the delay Δ is set to approximately 20% less than $1/4J_{XH}$ to reduce relaxation losses. A homospoil gradient pulse (HS) is applied, as shown, to reduce subtraction artefacts. In practice, composite heteronuclear 180° pulses of the form $90_x180_y90_x$ are used. Quadrature detection in the ω_1 dimension can be achieved by either the TPPI method or the hypercomplex method (see text).

Figure 8(b) shows the sensitivity-enhanced heteronuclear relay pulse sequence. A product operator analysis of the first part of this sequence has been given above for the HSQC experiment. The operators present following the second reverse INEPT sequence, just prior to the isotropic mixing period, are

$$+I_z \cos \omega_S t_1, \qquad -I_y \sin \omega_S t_1, \tag{65}$$

which are recognized as the orthogonal in-phase magnetization components required for the PEP method of sensitivity enhancement. These operators now pass into the isotropic mixing period. As discussed above, the isotropic mixing period gives rise to an effective Hamiltonian that is completely dominated by the scalar coupling interaction and commutes with any component of the total spin angular momentum. Thus evolution during the mixing period does not cause orthogonal magnetization components to mix. Coherence transfer occurs simultaneously and independently for the two terms in (65):

$$+I_z^c \cos \omega_S t_1 \rightarrow +I_z^r \cos \omega_S t_1 \tag{66}$$

via longitudinal magnetization, and

$$-I_y^c \sin \omega_S t_1 \rightarrow -I_y^r \sin \omega_S t_1 \tag{67}$$

via transverse magnetization, where I_k^c and I_k^r denote magnetization components of scalar-coupled I spins (protons) that are directly and remotely connected to the X spin (heteronucleus). At the end of the isotropic mixing the two orthogonal components are conserved. A final $90_y^\circ(I)$ pulse generates two observable terms of the forms (in addition to similar terms for the directly coupled protons)

$$+I_x^r \cos \omega_S t_1, \qquad -I_y^r \sin \omega_S t_1. \tag{68}$$

The accumulation of a second experiment with phase inversion of the 90° pulse on the heteronucleus immediately following the t_1 period generates the two observable terms

$$-I_x^r \cos \omega_S t_1, \qquad -I_y^r \sin \omega_S t_1. \tag{69}$$

Addition of the two data sets yields the single observable term

$$-2I_y^r \sin \omega_S t_1, \tag{70}$$

while subtraction on the other hand gives

$$-2I_x^r \cos \omega_S t_1. \tag{71}$$

The coefficient of 2 in (70) and (71) arises because two acquisitions have been used to produce them. Both the data sets represented by (70) and (71) can be phased to have pure absorption lineshapes in both dimensions. Addition of these phased spectra then yields a two-dimensional heteronuclear relay

spectrum in which, neglecting relaxation, the NMR resonances should be double in size. As has been described above, the noise increase from such a combination procedure is only $\sqrt{2}$, and a signal-to-noise ratio increase of $\sqrt{2}$ is expected compared with the conventional experiment. In practice, the sensitivity improvement is expected to be slightly less than $\sqrt{2}$ because of the previously analysed relaxation phenomena during the extended HSQC portion of the sequence.

5.2. Experimental demonstration

One of the most useful applications of the sensitivity-enhanced heteronuclear relay experiment is to provide through-bond correlations within each amino acid spin system in a protein, starting from the backbone amide. To demonstrate the experimental validity of the proposed enhanced sequence, two-dimensional heteronuclear relay spectra were acquired using the conventional sequence of Fig. 8(a) and the modified sequence of Fig. 8(b). Isotropic mixing was achieved using the DIPSI-2 sequence. The relevant phase-cycling information is given in the figure caption. All experiments were performed on a sample of the enzyme IIA^{glc}-like domain (previously referred to as enzyme III^{glc}) that was uniformly ^{15}N-labelled.[65] The total experimental time was 18 h for the conventional experiment and 18 h for the modified experiment.

For the conventional and ENHANCED spectra the r.m.s. baseline noise was calculated, and the intensities of 168 resolved relayed cross-peaks were determined. The ratio of the r.m.s. noise in the two spectra agreed with the expected value of $\sqrt{2}$. The average improvement in the signal-to-noise in the ENHANCED spectrum compared with the conventional spectrum was 1.27. As expected, the overall sensitivity enhancement is slightly less than the theoretical maximum of $\sqrt{2}$, owing to relaxation effects during the additional delays in the new pulse sequence. However, for a protein of this size (17.4 kDa) this is not surprising, and still represents a significant increase.

As in the cases described earlier, in addition to the conventional spectrum, ADD, SUBTRACT and ENHANCED spectra are shown in Fig. 9 for comparison purposes. The figure shows slices taken parallel to the ω_2 dimension through selected resonances of the two-dimensional spectra. Each cross-section shows the resonances through which magnetization has been relayed from the amide proton by the DIPSI-2 mixing sequence. The relevant ^1H assignments are noted on the figure; the ^{15}N frequency in each case is that of the backbone amide of that particular residue. As can be seen the ADD and SUBTRACT spectra are virtually identical to the conventional spectrum and the signal-to-noise ratio of the ENHANCED spectrum is superior to that of the conventional heteronuclear relay spectrum. Note that the slices are plotted on an absolute scale to show the increase in noise size for the ENHANCED spectrum compared to the others.

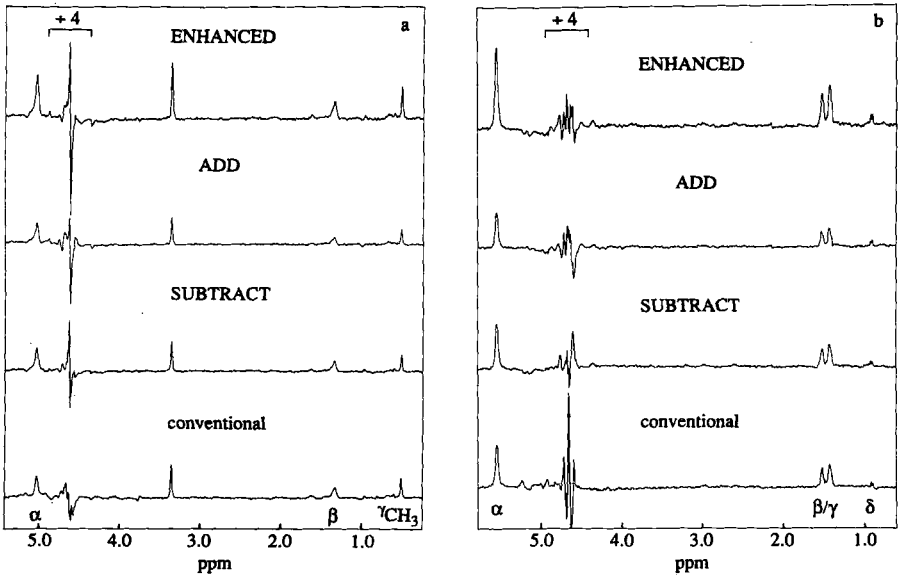

Fig. 9. Conventional and sensitivity-enhanced heteronuclear relay spectra of enzyme III^{glc}. All experiments were performed on a sample of the enzyme III^{glc}-like domain from *Bacillus subtilis* (0.8 mM, 90% H_2O/10% D_2O, pH 6.6 10 mM kP_i, 308 K), a 162-residue protein (MW = 17 400) that was uniformly labelled with $^{15}N > 95\%$.[65] Spectroscopy was performed on a Bruker AM600 spectrometer equipped with an Aspect 3000 computer and digital phase-shifting hardware. Data processing was performed using software supplied by Hare Research. The conventional heteronuclear relay spectrum was acquired using the pulse sequence of Fig. 8(a) and a Hahn echo. Sixty-four scans were acquired per t_1 increment. The two data sets required to produce the sensitivity-enhanced spectrum were acquired using the pulse sequence of Fig. 8(b) and a Hahn echo.[66,67] Each data set was acquired with 32 scans per t_1 increment. For all spectra, 4K real data points (2K per quadrature channel) were acquired in t_2 and 448 real points were acquired in t_1. TPPI was used for frequency discrimination in the ω_1 dimension. The spectral width was 12 500 Hz in the ω_2 dimension and 3333 Hz in the ω_1 dimension. The proton carrier was placed on the H_2O resonance and the ^{15}N carrier was placed at 107.5 ppm. The delay Δ was set to 2.3 ms. The homospoil gradient pulse was 3 ms, and was followed by a 7 ms delay to allow the magnetic field to stabilize. The two data sets acquired using the sequence of Fig. 8(b) were alternately added and subtracted to produce the two new data sets, called ADD and SUBTRACT respectively, which were then used for subsequent data reduction. Spectra were processed using exponential weighting in ω_2 and a

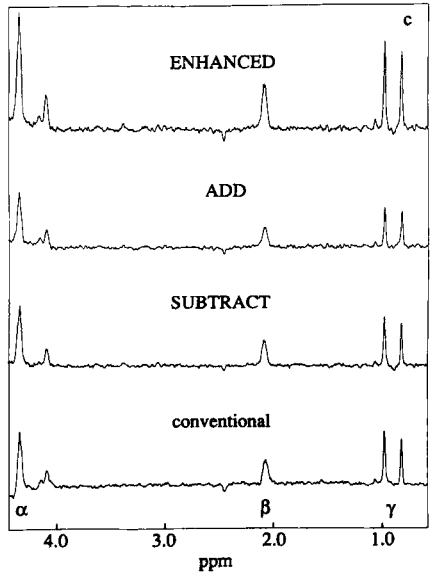

Kaiser window in ω_1. Prior to Fourier transformation, the data were zero-filled to 8K and 4K real points in t_2 and t_1 respectively. The conventional and SUBTRACT were phased to be purely absorptive in both dimensions; the ADD spectrum was also phased to be purely absorptive by adding a 90° phase shift in both dimensions relative to the SUBTRACT spectrum. The cross-sections shown are parallel to the ω_2 axis at the backbone amide ^{15}N shift in ω_1 for (a) Ile 80, (b) Leu 113 and (c) Val 63.[65] In each case the bottom trace is taken from the conventional heteronuclear relay spectrum, the second trace from the SUBTRACT spectrum, the third trace from the ADD spectrum, and the top trace from the ENHANCED spectrum. The slices are plotted on the same absolute intensity scale; as indicated, the intensities of the residual water resonances in (a) and (b) have been reduced by a factor of four. For each spin system the peaks resulting from the relay of magnetization from the amide proton are noted; the amide resonances are not shown. Peaks that are from other spin systems are not labelled. As expected, the conventional spectrum, the ADD spectrum, and the SUBTRACT spectrum are nearly identical in all cases. The sensitivity enhancement for a given peak in the ENHANCED spectrum compared to the conventional spectrum is calculated as the ratio of the relative peak intensities to the theoretical increase in the r.m.s. baseline noise, $\sqrt{2}$, for the two spectra. The average enhancements for each of the spin systems shown are (a) 1.27, (b) 1.28 and (c) 1.25.

6. SENSITIVITY IMPROVEMENT IN THREE-DIMENSIONAL HETERONUCLEAR CORRELATION SPECTROSCOPY

Three-dimensional NMR spectroscopy has been shown to offer significant improvements in spectral resolution compared with the 2D techniques commonly employed for biomolecular structural investigations. Combining two of the most powerful two-dimensional homonuclear methods for structure elucidation (TOCSY and NOESY) with the resolving power of the (generally) larger chemical-shift dispersion of ^{13}C and ^{15}N heteronuclei into three-dimensional experiments has proved a remarkably successful procedure for alleviating resonance overlap.[68–71]

The application of PEP technology to achieve sensitivity improvements of up to $\sqrt{2}$ in the 3D TOCSY–HMQC[68] and 3D NOESY–HMQC[72–74] experiments is demonstrated in Sections 6.1 and 6.2. The same enhancement can, of course, be obtained in the HSQC versions of these experiments.

6.1. 3D TOCSY–HMQC

The same pulse sequence, shown in Fig. 10(a), is used for the conventional and sensitivity-enhanced (SE) TOCSY–HMQC experiments. The principle of the method can be seen for a spin system consisting of two scalar-coupled protons A and B, with their mutual coupling constant denoted by J, and a heteronucleus S that is scalar-coupled to at least one of the protons, say B, with a one-bond coupling constant J_{SB}. Beginning with equilibrium magnetization of the A spin, evolution of coherence during the pulse sequence is easily followed by using the product operator formalism. Coherence transfer from proton A to proton B occurs independently during the isotropic mixing period for the two orthogonal single-spin operators present following the t_1 period:

$$-\text{sgn}(\phi_2)\, A_z \cos \omega_A t_1 \cos \pi J t_1 \rightarrow -\text{sgn}(\phi_2)\, B_z \cos \omega_A t_1 \cos \pi J t_1, \quad (72)$$

$$A_x \sin \omega_A t_1 \cos \pi J t_1 \rightarrow B_x \sin \omega_A t_1 \cos \pi J t_1, \quad (73)$$

in which ω_A is the resonance frequency of the A spin, t_1 is the duration of the first incrementable time period, and sgn (ϕ_2) is the sign of the initial phase for ϕ_2. One-half of the number of transients recorded per increment is obtained with sgn $(\phi_2) = 1$ and the other half is obtained with sgn $(\phi_2) = -1$ by inverting the phase ϕ_2. Multi-spin terms have been excluded for the usual reasons. Again, we assume complete coherence transfer to occur from spin A to spin B.

Concentrating on the B-proton terms, the remainder of the pulse sequence constitutes an HMQC isotope filter. The B-operator terms in (72) and (73) are labelled with the chemical shift of the heteronucleus, ω_S, during t_2;

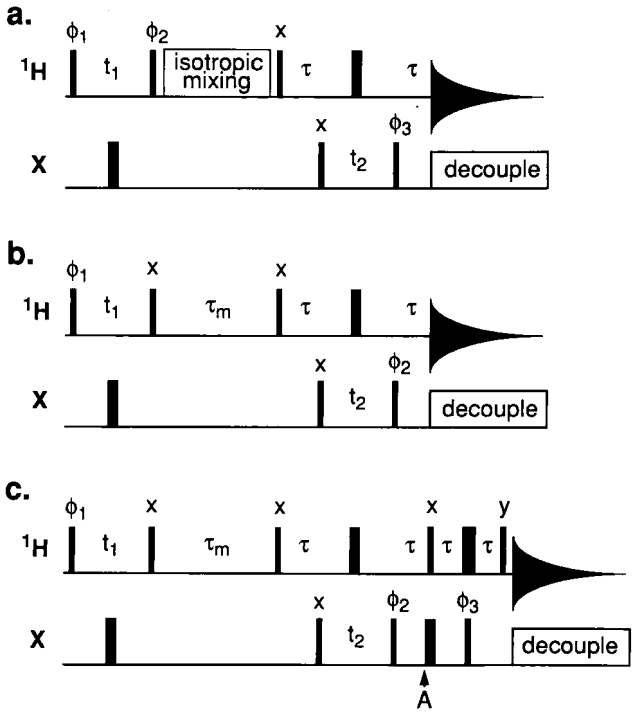

Fig. 10. Pulse sequences for recording three-dimensional (a) conventional and SE–TOCSY–HMQC, (b) conventional NOESY–HMQC, and (c) SE–NOESY–HMQC experiments. The thin and thick vertical lines represent 90° and 180° pulses applied to the H (protons) or X (heteronucleus) spins; the delay τ is set to $1/2J_{XH}$. Decoupling is accomplished by an appropriate composite pulse sequence. Quadrature detection in the ω_1 dimension can be achieved by either the TPPI method or the hypercomplex method. Isotropic mixing is achieved by DIPSI-2 or a similar pulse scheme. The basic phase cycle for (a) is $\phi_1 = (x, -x)$, $\phi_2 = x$, $\phi_3 = (x, x, -x, -x)$ and receiver = $(x, -x, -x, x)$. For the conventional TOCSY–HMQC experiment the phases of ϕ_2 and the receiver are inverted after four scans. For the SE–TOCSY–HMQC experiment the phase of ϕ_2 is inverted after four scans, and the two halves of the data are stored separately. The basic phase cycle for (b) is $\phi_1 = (x, -x)$, $\phi_2 = (x, x, -x, -x)$ and receiver = $(x, -x, -x, x)$. The basic phase cycle for (c) is $\phi_1 = (x, -x)$, $\phi_2 = (x, x, -x, -x)$, $\phi_3 = (y, y, -y, -y)$ and receiver = $(x, -x, -x, x)$. In (c) the phase of ϕ_2 is inverted after four scans, and the two halves of the data are stored separately.

consequently the observable terms detected during the acquisition period t_3 are

$$\tfrac{1}{2}(-B_y \cos \omega_A t_1 + B_x \sin \omega_A t_1) \cos \pi J t_1 \cos \omega_S t_2 \cos \pi J t_2 \tag{74}$$

for the data acquired with sgn $(\phi_2) = 1$, and

$$\tfrac{1}{2}(B_y \cos \omega_A t_1 + B_x \sin \omega_A t_1) \cos \pi J t_1 \cos \omega_S t_2 \cos \pi J t_2 \tag{75}$$

for the data acquired with sgn $(\phi_2) = -1$.

In the conventional TOCSY–HMQC experiment the two halves of the data represented by (74) and (75) are subtracted by inverting the phase of the receiver in synchrony with ϕ_2. The recorded signal is then given by

$$-B_y \cos \omega_A t_1 \cos \pi J t_1 \cos \omega_S t_2 \cos \pi J t_2. \tag{76}$$

The data represented by (76) can be Fourier-transformed to give a 3D spectrum with absorptive lineshapes in all three dimensions. In the SE–TOCSY–HMQC experiment the two halves of the data are recorded separately. Subsequently the two data sets are alternately added to give

$$B_x \sin \omega_A t_1 \cos \pi J t_1 \cos \omega_S t_2 \cos \pi J t_2, \tag{77}$$

and subtracted to yield the same result as (76). The data set represented by (77) is 90° out of phase with respect to that of (76), in the t_1 and t_3 periods, but both can be individually phased to generate two 3D TOCSY–HMQC with pure absorption lineshapes in all three dimensions. The spectra would have the form of homonuclear TOCSY spectra correlating A and B spins, separated by the chemical shift of the appropriate heteronucleus S.

Addition of the two 3D data sets doubles the size of the resonances, while the r.m.s. noise increases only by the factor of $\sqrt{2}$, and a sensitivity improvement of $\sqrt{2}$ is obtained compared with the conventional method.[75]

6.2. 3D NOESY–HMQC

A similar approach can be used to obtain sensitivity enhancement of the 3D NOESY–HMQC experiment; however, modification of the conventional pulse sequence is required.[75] Figures 10(b, c) show the 3D conventional and SE–NOESY–HMQC pulse sequences respectively. The principles of the experiment can be illustrated for a system of two protons A and B that are close enough in space to cross-relax via their mutual dipolar interaction. The heteronucleus S is again scalar coupled to proton B.

Beginning with equilibrium magnetization of the A spin, the product-operator term of interest following the t_1 period cross-relaxes with proton B during the mixing period to give

$$-A_z \cos \omega_A t_1 \cos \pi J t_1 \rightarrow -B_z \cos \omega_A t_1 \cos \pi J t_1 \tag{78}$$

for molecules in the slow motion limit. For the conventional experiment (Fig. 10b) the remainder of the pulse sequence comprises an HMQC isotope filter. The final detectable term is

$$-B_y \cos \omega_A t_1 \cos \pi J t_1 \cos \omega_S t_2, \tag{79}$$

which yields a 3D NOESY–HMQC spectrum with pure absorptive lineshapes in all dimensions.

For the SE–NOESY–HMQC sequence the isotope filter extends to the point labelled A in Fig. 10(c), at which the operators present are

$$[-\text{sgn}(\phi_2)\, B_y \cos \omega_S t_2 + B_x \sin \omega_S t_2\, (S_x \cos \omega_S \tau + S_y \sin \omega_S \tau)] \cos \omega_A t_1 \cos \pi J t_1. \tag{80}$$

One-half of the number of transients per t_2 increment is recorded with each value of sgn (ϕ_2). During the remainder of the sequence, the second term in (80) is refocused to a single-quantum proton operator. The resultant observable operators immediately prior to acquisition are

$$\tfrac{1}{2}(-B_x \cos \omega_S t_2 - \delta_{1N} B_y \sin \omega_S t_2) \cos \omega_A t_1 \cos \pi J t_1 \tag{81}$$

for the data acquired with sgn $(\phi_2) = 1$, and

$$\tfrac{1}{2}(B_x \cos \omega_S t_2 - \delta_{1N} B_y \sin \omega_S t_2) \cos \omega_A t_1 \cos \pi J t_1 \tag{82}$$

for the data acquired with sgn $(\phi_2) = -1$. The Kronecker delta δ_{1N} is used to indicate that the second term in (80) can be refocused only for heteronuclei with $N = 1$ directly attached protons. The two halves are alternately added to yield

$$-\delta_{1N} B_y \sin \omega_S t_2 \cos \omega_A t_1 \cos \pi J t_1 \tag{83}$$

and subtracted to yield

$$-B_x \cos \omega_S t_2 \cos \omega_A t_1 \cos \pi J t_1. \tag{84}$$

The two data sets represented by (83) and (84) are 90° out of phase with respect to each other in the t_2 and t_3 periods, and are in-phase in the t_1 period. As before for the PEP method, the two data sets can be processed independently to give purely absorptive lineshapes in all three dimensions. Addition of the two spectra yields an overall signal-to-noise increase of up to $\sqrt{2}$ in the enhanced spectrum for heteronuclei with a single directly attached proton, compared with the conventional NOESY–HMQC experiment. As described above, the actual improvement in the 3D SE–NOESY–HMQC experiment will be slightly less than the theoretical value of $\sqrt{2}$ due to relaxation effects during the longer pulse sequence of Fig. 10(c). As in the 2D experiments, the data can also be combined in the time-domain according to the PEP prescription of Section 2.3.1, provided that the hypercomplex

method has been employed for frequency discrimination in the affected dimension.

6.3. Experimental demonstration

The above analysis was verified experimentally by recording ^{1}H–^{15}N–^{1}H 3D conventional and sensitivity-enhanced TOCSY–HMQC and NOESY–HMQC spectra using the pulse sequences given in Figs 10(a–c). Experiments were performed on a 2.5 mM solution of calbindin D_{9k} in 90% H_2O/10% D_2O at 300 K. Calbindin D_{9k} is a 75 amino acid calcium-binding protein;[76] the sample used for NMR studies was uniformly labelled with ^{15}N to >95%. Examples of the processed 3D spectra obtained for the TOCSY–HMQC and NOESY–HMQC experiments are shown in Figs 11 and 12 respectively. Figure 11 illustrates the sensitivity improvement obtained for TOCSY transfer through the spin systems of Lys 12 and Glu 35 in calbindin D_{9k}. The experimentally measured increase in sensitivity between the enhanced and conventional TOCSY–HMQC spectra are 42% for Lys 12 and 38% for Glu 35, across the whole spin system. Figure 12 illustrates the sensitivity improvement obtained for magnetization transfer via cross-relaxation with the amide proton of the spin systems of Lys 12 and Glu 35 is calbindin D_{9k}. The average enhancement across each cross-section in Fig. 12(a) is 41% while that across the cross-section of Fig. 12(b) is 39%. The enhancement for the SE–TOCSY–HMQC experiment agrees well with the theoretical value of $\sqrt{2}$, as expected since the pulse sequence remains unmodified. Although in the case of the SE–NOESY–HMQC experiment, a $\sqrt{2}$ improvement in signal-to-noise ratio is also seen, this is unlikely always to be the case. The pulse sequence for this experiment has been extended from the conventional sequence, and relaxation effects will become more important as the biomolecule under investigation becomes larger. As noted earlier, sensitivity enhancement is most strongly affected by relaxation in experiments that use the HMQC isotope filter; consequently, for proteins larger than calbindin the SE–NOESY–HSQC experiment may be preferable.

7. SENSITIVITY IMPROVEMENT IN PROTON-DETECTED HETERONUCLEAR SPIN RELAXATION MEASUREMENTS

An expanding body of theoretical and experimental results indicate that intramolecular, dynamical processes are intimately involved in protein function.[77–80] Furthermore, the interpretation of NMR data used to generate constraints for structure calculations should ideally encompass intramolecular dynamics.[81–83] Dipolar nuclear magnetic spin relaxation of

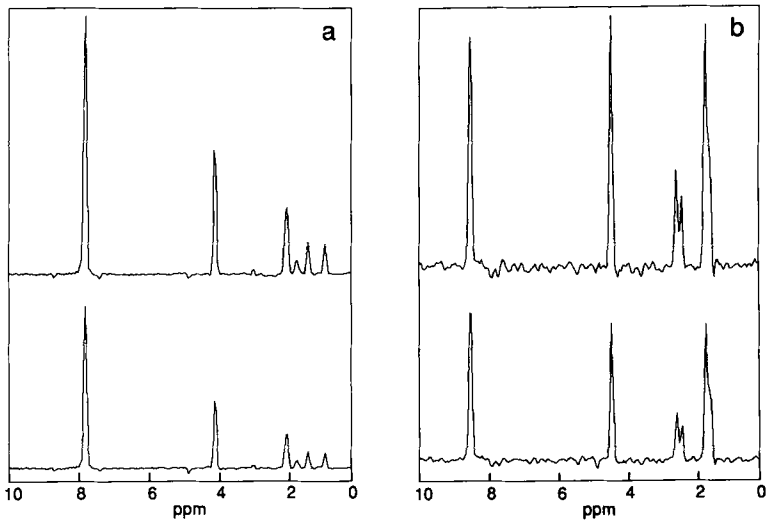

Fig. 11. Comparison of conventional and SE–TOCSY–HMQC spectra recorded on the ^{15}N-enriched calcium binding protein calbindin (see text). A single data set was recorded on a Bruker AM600 spectrometer with the pulse sequence of Fig. 10(a). The conventional spectrum was obtained by subtracting the two halves of the data set represented by (67) and (68) after acquisition. A total of eight transients were recorded per (t_1, t_2) data point; the data matrix consisted of $256 \times 64 \times 2048$ real points in the $t_1 \times t_2 \times t_3$ dimensions respectively. The spectral widths were 7812 Hz in the t_1 and t_3 proton dimensions and 1506 Hz in the t_2 nitrogen dimension. The isotropic mixing period was 60 ms. The cross-sections shown are taken from the 3D TOCSY–HMQC spectra parallel to the ω_1 axis at the ω_2, ω_3 frequencies of the backbone amide ^{15}N and proton resonances for the spin systems of (a) Lys 12 and (b) Glu 35. The top and bottom traces show sensitivity-enhanced and conventional spectra respectively. The spectra are plotted on an absolute intensity scale, and it is noted that the increase in the r.m.s. baseplane noise seen here for the enhanced spectrum compared with the conventional one agrees with the theoretical value of $\sqrt{2}$. The average signal-to-noise improvements between the enhanced and conventional spectra are (a) 1.42 and (b) 1.38.

protonated heteronuclei, such as ^{13}C and ^{15}N, is mediated by overall rotational tumbling of the molecule and by internal motions of X—H bond vectors;[84] consequently, heteronuclear NMR spectroscopy is a powerful technique for experimental investigation of dynamics in biological macromolecules.[85] The measurement of spin–lattice and spin–spin relaxation rate constants (R_1 and R_2 respectively) and the steady-state {^{1}H}–X nuclear Overhauser effect (NOE), is proving to be viable for a growing number of proteins.[51–53,86–95]

Basic methods for the determination of X-nucleus relaxation parameters by proton-detected heteronuclear correlation experiments have been described elsewhere,[51–53,96,97] as have techniques for minimizing systematic

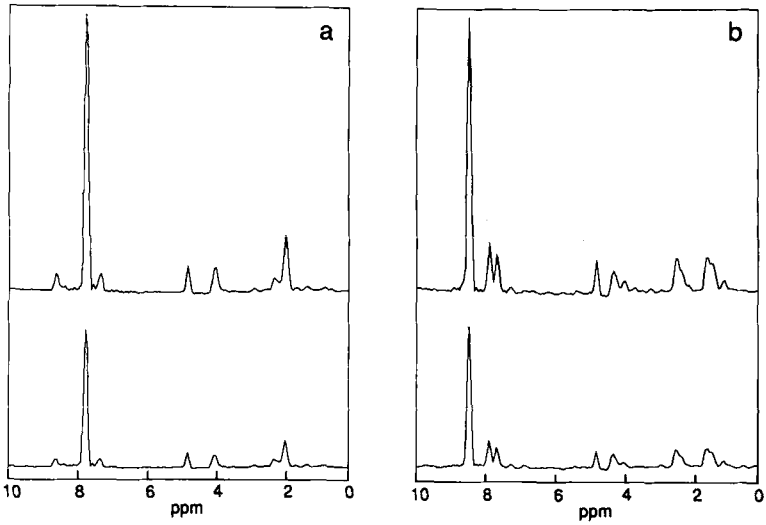

Fig. 12. Comparison of conventional and SE–NOESY–HMQC spectra recorded on the ^{15}N-enriched calcium binding protein calbindin (see text). The data sets were recorded on a Bruker AMX500 spectrometer using the pulse sequences of Figs 10(b, c). A total of 16 transients were recorded per (t_1, t_2) data point; the data matrix consisted of 100 complex × 32 complex × 2048 real points in the $t_1 \times t_2 \times t_3$ dimensions respectively. The spectral widths were 7042 Hz in the t_1 and t_3 proton dimensions and 1250 Hz in the t_2 nitrogen dimension. The NOESY mixing time was 150 ms. Both experiments were recorded in the same overall time. The cross-sections shown are taken from the 3D NOESY–HMQC spectra parallel to the ω_1 axis at the ω_2, ω_3 frequencies of the backbone amide ^{15}N and proton resonances for the spin systems of (a) Lys 12 and (b) Glu 35. The top and bottom traces show sensitivity-enhanced and conventional spectra respectively. The spectra are plotted on an absolute intensity scale, and it is noted that the increase in the r.m.s. baseplane noise seen here for the enhanced spectrum compared with the conventional one agrees with the theoretical value of $\sqrt{2}$. The average signal-to-noise improvements between the enhanced and conventional spectra are (a) 1.41 and (b) 1.39.

contributions from dipole–CSA cross-correlation effects,[98–100] and from evolution of antiphase terms during R_2 measurements.[98,99,101]

7.1. Theory

Using the same principles as described and demonstrated above for increasing the signal-to-noise ratio in heteronuclear correlation experiments, it is possible to enhance the sensitivity of heteronuclear relaxation methods for AX systems.[87,91,102]

The modified pulse schemes used to measure R_1, R_2 and the {^{1}H}–XNOE, along with the conventional sequence to measure R_1, are shown in

Fig. 13 (although in the figure ^{15}N is shown as the heteronucleus, the sequences are, of course, applicable to other heteronuclei, such as ^{13}C). As in the other cases, the R_1 and R_2 sensitivity-enhancement sequences consist of an initial refocused INEPT transfer from ^1H to X, the relaxation period t, the t_1 evolution period, and the now familiar extended reverse polarization transfer scheme that allows phase-sensitive detection of the orthogonal magnetization components produced during t_1. Proton decoupling is performed using a composite pulse decoupling sequence during the relaxation delay of the inversion recovery sequence (Fig. 13b) to suppress the time-dependent effects of dipolar X–^1H cross-relaxation and of cross-correlation between dipolar and CSA relaxation mechanisms.[100] In order to suppress the time-dependent effects of cross-correlation between dipolar and CSA relaxation mechanisms in the CPMG experiments (Fig. 13c), proton decoupling is performed using synchronous proton 180° hard pulses during the relaxation delay t.[98,99] The spin-echo delay in CPMG experiments must be short to minimize effects from evolution under the heteronuclear scalar coupling Hamiltonian; $\tau = 0.5$ ms is sufficient for this purpose.[99] Inversion recovery and CPMG[103,104] decay curves are obtained by recording a series of 2D heteronuclear correlation spectra in which the relaxation period t is varied parametrically. The steady-state NOE[105] pulse sequence consists of the t_1 evolution period and the extended reverse polarization transfer segment. The NOE enhancements are measured by recording pairs of spectra with and without saturation of protons during the recycle time between transients (Fig. 13d). Saturation of protons during the recovery delay is performed using a composite pulse decoupling sequence. In all sequences the H_2O resonance is suppressed by short spin-lock purge pulses during the INEPT transfer steps to minimize the effects of saturation transfer from the solvent protons.[106]

In the sensitivity-enhancement heteronuclear correlation sequences two data sets are recorded differing only by inversion of the phase of the first heteronuclear pulse after the t_1 period (Figs 13b–d). If each data set is recorded with n scans per increment, two independent pure-phase spectra with $2n$ scans per increment are obtained by adding and subtracting the recorded data, as described above. The peak intensities in the spectra obtained by addition (I^a) and subtraction (I^s) of the recorded data sets are given by

$$I^a = I^c\varepsilon_a = I^c \exp(-2R_1\Delta), \tag{85}$$

$$I^s = I^c\varepsilon_s = I^c \exp(-2R_1^H\Delta), \tag{86}$$

in which I^c is the intensity that would be obtained in the equivalent conventional experiment, ε_a and ε_s are the fractional losses of signal due to the additional delays and pulses in the enhanced sequences compared with the conventional experiments, R_1 is the ^{15}N spin–lattice relaxation rate

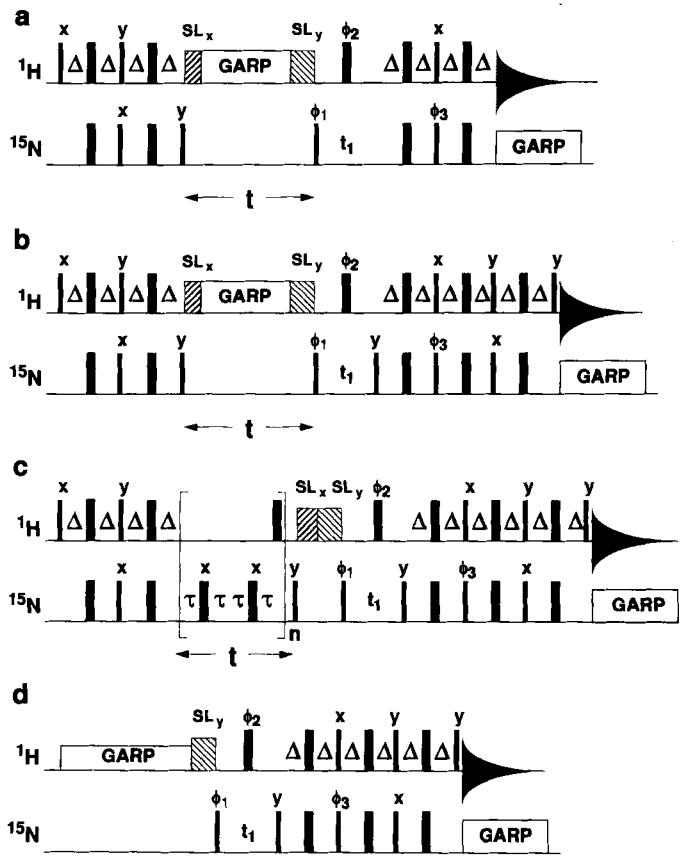

Fig. 13. Pulse schemes used to measure (a, b) ^{15}N R_1, (c) ^{15}N R_2 and (d) $\{^1H\}$–^{15}N NOE with indirect proton detection. Sensitivity enhancement schemes are shown in (b)–(d) and the conventional inversion recovery sequence is shown in (a). Thin bars represent 90° pulses and thick bars 180° pulses. The phase cycling used for R_1 and R_2 experiments is $\phi_1 = (x, -x, x, -x)$, $\phi_2 = (y)_4(-y)_4$, $\phi_3 = (y, y, -y, -y)$ and receiver = $(x, -x, -x, x)$. In the case of the $\{^1H\}$–^{15}N NOE experiments the following phase cycle is suggested: $\phi_1 = (x, -x, x, -x, -x, x, -x, x)_2$, $\phi_2 = (y)_{16}(-y)_{16}$, $\phi_3 = (y, y, -y, -y)_2(-y, -y, y, y)_2$ and receiver = $(x, -x, -x, x, -x, x, x, -x, -x, x, x, -x, x, -x, -x, x)$. In all cases, for sensitivity enhancement, each t_1 experiment is recorded twice with the phase of the ^{15}N 90° pulse immediately after t_1 differing by 180°. Linear combination of these two experiments produces sensitivity enhancement. The 180° pulses without phase designations are applied along the y axis. The value of Δ is set to $1/4J_{NH}$. For (a), (b) and (c) the delay t is parametrically varied in a series of 2D experiments; for (d) pairs of spectra are acquired with and without proton saturation.

constant, R_1^H is the proton spin–lattice relaxation rate constant, $\Delta = 1/4J$, and J is the one-bond N—H scalar coupling constant. The second equalities in (85) and (86) are obtained if the effects of pulse imperfections are negligible. For the inversion recovery and CPMG experiments I^a and I^s are combined to yield

$$I(t) = [I_\infty^c - (I_\infty^c - I_0^c)\exp(-t/R_1)](\varepsilon_a + \varepsilon_s) = I_\infty - (I_\infty - I_0)\exp(-t/R_1), \quad (87)$$

$$I(t) = [I_0^c \exp(-t/R_2) + I_\infty^c](\varepsilon_a + \varepsilon_s) = I_0 \exp(-t/R_2) + I_\infty \quad (88)$$

respectively. In (87) and (88) I_0 is the peak intensity for $t = 0$ while I_∞ is the limiting peak intensity as $t \to \infty$. Peak intensities may decay to a non-zero limiting value in CPMG experiments as a consequence of pulse imperfections.[107] Thus the time series for both experiments have the same forms as for the conventional experiments; however, the signal-to-noise ratio in the final enhanced spectrum is proportional to $[2n(\varepsilon_a + \varepsilon_s)]^{1/2}$, unlike the conventional case where it is proportional to $(2n)^{1/2}$. Since $2R_1\Delta \ll 1$ and $2R_1^H\Delta \ll 1$ for proteins with molecular masses less than 20 kDa, $\varepsilon_a + \varepsilon_s \approx 2$ and the signal-to-noise ratio in the enhanced spectrum is nearly equivalent to that in a conventional experiment acquired with $4n$ scans per increment. For the NOE experiments the NOE is calculated independently for the ADD and SUBTRACT linear combinations of data sets:

$$\text{NOE} = \frac{I_{sat}^a}{I_{unsat}^a} = \frac{I_{sat}^s}{I_{unsat}^s} = \frac{I_{sat}}{I_{unsat}}, \quad (89)$$

in which I_{sat} and I_{unsat} are the peak intensities in spectra recorded with and without saturation of protons during the recycle delay. Thus two independent measurements of the NOE enhancement are obtained in the same time required for a single conventional measurement with the same total number of scans per increment. Alternatively, the data can be combined as usual to yield a sensitivity-improved spectrum.

As a consequence of incorporating PEP technology, relaxation data with a given signal-to-noise ratio can be acquired in approximately one-half of the measurement time required by the conventional pulse sequences.[102]

7.2. Experimental demonstration

To demonstrate the sensitivity improvement that can be achieved by applying PEP technology in heteronuclear relaxation experiments, data are shown in Fig. 14 for a sample of the Pro43Gly mutant of calbindin D_{9k} (in D_2O) that has been uniformly isotropically enriched in ^{13}C to a level of approximately 15% abundance. The data (Rance, Chazin and Palmer, unpublished results) presented in Fig. 14 are 1D slices (displaying proton

chemical shifts) taken from 2D ^{1}H–^{13}C heteronuclear correlation spectra recorded using the T_1 pulse sequence of Fig. 13(b); the inversion–recovery delay for these data was 1.06 s. The top slice was taken from a spectrum in which the two separately collected data sets (for the two halves of the phase cycle) were added together, the middle slice from the spectrum for the subtracted data (with a 90° phase correction in both dimensions relative to the "add" spectrum), and the bottom slice from the composite spectrum in which the "add" and "subtract" have been combined. The slices intersect peaks for the $^{\alpha}C^{\alpha}H$ correlations of Val 61 (5.10 ppm), Thr 45 (4.43 ppm), Tyr 13 (4.00 ppm) and Lys 25 (3.46 ppm). The three slices are plotted on a scale such that the r.m.s. noise levels are the same, which required the composite slice to be reduced by a factor of $\sqrt{2}$ relative to the component slices, as expected on theoretical grounds. The data in Fig. 14 clearly demonstrate the improved sensitivity afforded by incorporating PEP technology into the heteronuclear relaxation experiments.

8. SENSITIVITY ENHANCEMENT IN GRADIENT-ENHANCED HETERONUCLEAR CORRELATION SPECTROSCOPY

Until recently, the selection of desired coherence transfer pathways[108,109] in solution-state NMR experiments has relied almost solely on the use of phase-cycling procedures or radiofrequency pulse inhomogeneity to eliminate unwanted pathways. In principle, a third alternative—pulsed magnetic field gradient technology—also provides a very powerful means for coherence transfer pathway selection, but was seldom employed in NMR spectroscopy in the past owing to hardware limitations. However, recent developments in probe technology and related hardware have greatly facilitated the use of pulsed field gradients, and as a result a number of new or improved experiments have been proposed that rely on gradient methodology. These developments are very important because of the significant advantages offered by gradient methodology for coherence pathway selection. One of the principal advantages is that pathway selection can be achieved within a single scan, as opposed to the multiple scans required for phase-cycling procedures. In addition, an extremely important advantage in biological applications in aqueous solution is the possibility of suppressing the enormous water resonance with appropriate field gradients in a single scan; alternative methods for solvent suppression are usually compromised by problems with saturation transfer, non-uniform spectra excitation or dynamic range limitations in the receiver.

Recently, Kay and co-workers[110] have incorporated PEP technology into a pulsed field gradient variation of the HSQC experiment. Their new method allows pure absorption heteronuclear correlation spectra to be recorded with the use of pulsed field gradients for eliminating undesired

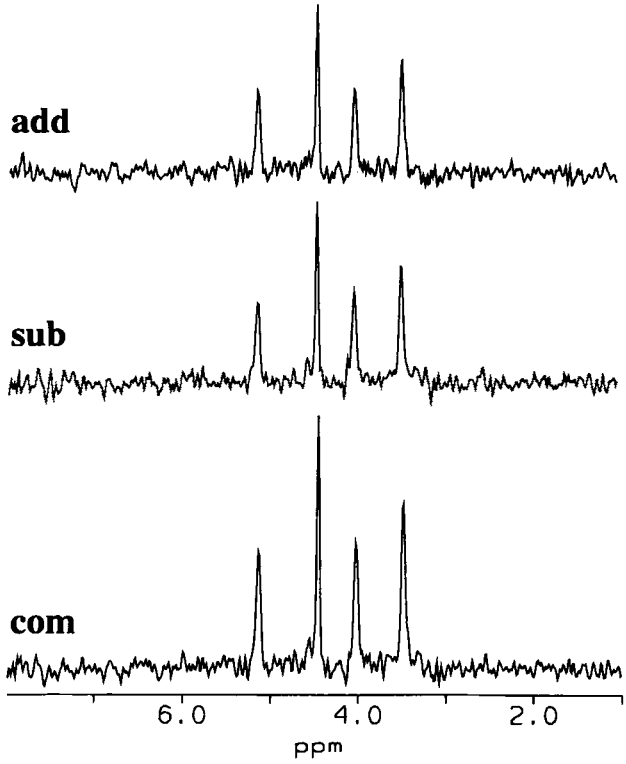

Fig. 14. One-dimensional slices (displaying proton chemical shifts) taken from 2D ^{1}H–^{13}C heteronuclear correlation spectra recorded using the T_1 pulse sequence of Fig. 13(b); the inversion-recovery delay for these data was 1.06 seconds. The top slice was taken from a spectrum in which the two separately collected data sets (for the two halves of the phase cycle) were added together, the middle slice from the spectrum for the subtracted data (with a 90° phase correction in both dimensions relative to the "add" spectrum), and the bottom slice from the composite spectrum in which the "add" and "subtract" have been combined. The slices intersect peaks for the $^{\alpha}C^{\alpha}H$ correlations of Val 61 (5.10 ppm), Thr 45 (4.43 ppm), Tyr 13 (4.00 ppm) and Lys 25 (3.46 ppm). The three slices are plotted on a scale such that the r.m.s. noise levels are the same, which required the composite slice to be reduced by a factor of $\sqrt{2}$ relative to the component slices, as expected on theoretical grounds.

coherence transfer pathways; in particular, the advantage of suppressing the water with field gradients is clearly demonstrated. This gradient-enhanced experiment employs a pulse sequence similar to that discussed in detail in Section 4.1 for the sensitivity-enhanced non-gradient HSQC experiment. PEP technology is employed in the gradient-enhanced experiment to extract separate signals, which are cosine- and sine-modulated as a function of the evolution time t_1; these data are then used to generate a hypercomplex data set, which can be Fourier-transformed to yield a pure absorption spectrum with

ω_1 frequency discrimination. Kay *et al.* demonstrate that the use of both PEP and gradient technology can yield significant improvements in sensitivity for moderately sized proteins or other biomolecules.

9. ADDITIONAL APPLICATIONS

The PEP technology for sensitivity enhancement can be incorporated into a wide variety of NMR experiments; two papers have appeared recently describing additional applications. Madsen and Sørensen[111] have described very useful modifications to a variety of "constant-time" experiments to achieve optimum spectral resolution. The general principle of a "constant-time" experiment was first presented by Bax and co-workers[112] as a means of eliminating homonuclear scalar couplings in the indirectly detected frequency dimension of 2D correlated spectra. This principle has found important applications in many recent 2D and 3D heteronuclear NMR experiments of uniformly ^{13}C-enriched biomolecules. PEP technology for sensitivity enhancement was incorporated into the optimized "constant-time" experiments presented by Madsen and Sørensen in a straightforward manner following the principles described by Palmer *et al.*[22] and reviewed above.

The application of PEP technology in a homonuclear, 3D NOESY–TOCSY experiment has recently been described by Feng Ni.[113] In this experiment a NOESY element is simply prefixed to the sensitivity-improved TOCSY experiment described by Cavanagh and Rance.[23]

10. CONCLUSIONS

This report has described the basic principle of a general methodology for improving the sensitivity of a variety of multidimensional NMR experiments, and has discussed the means by which this so-called PEP technology can be incorporated into some of the most popular experiments in current use. The basic requirement that must be satisfied in order to incorporate PEP technology into a multidimensional NMR experiment is that the orthogonal magnetization components present during an evolution period be made to follow approximately equivalent coherence transfer pathways during the subsequent portion of the pulse sequence. It should be anticipated that PEP technology will be applicable in additional classes of experiments not specifically addressed in this chapter. The maximum achievable improvement in sensitivity (defined as signal-to-noise ratio per unit measuring time) for PEP technology applied to one evolution period of a multidimensional NMR experiment is $\sqrt{2}$. Such improvement is extremely important in applications where the sensitivity is limited by practical factors

such as low sample concentrations or inherent features such as the requirement for large numbers of experiments in 3D and 4D experiments or in relaxation rate measurements.

ACKNOWLEDGEMENTS

The authors wish to acknowledge the fundamental contributions of Professor A. G. Palmer III, who was a principal architect of the sensitivity-improved heteronuclear NMR experiments, and Dr R. A. Byrd. Professor L. E. Kay is thanked for providing a preprint of ref. 110. A very helpful discussion with Professor G. Bodenhausen in which he pointed out a useful definition of sensitivity as "signal-to-noise ratio per unit time" is acknowledged. The preparation of this report was supported in part by a grant from the National Institutes of Health (GM 40089).

REFERENCES

1. D. I. Hoult, *Prog. NMR Spectrosc.*, 1978, **12**, 41.
2. O. W. Sørensen, *Prog. NMR Spectrosc.*, 1989, **21**, 503.
3. A. Bax, S. W. Sparks and D. A. Torchia, *Meth. Enzymol.*, 1989, **176**, 134.
4. R. R. Ernst, *Adv. Magn. Reson.*, 1966, **2**, 1.
5. M. H. Levitt, G. Bodenhausen and R. R. Ernst, *J. Magn. Reson.*, 1984, **58**, 462.
6. M. A. Delsuc and J. Y. Lallemand, *J. Magn. Reson.*, 1986, **69**, 504.
7. (a) M. H. Levitt and R. Freeman, *J. Magn. Reson.*, 1980, **39**, 533.
   (b) J. C. J. Barna, E. D. Laue, M. R. Mayger, J. Skilling and S. J. P. Worrall, *J. Magn. Reson.*, 1987, **73**, 69.
8. R. R. Ernst, G. Bodenhausen and A. Wokaun, *Principles of Nuclear Magnetic Resonance in One and Two Dimensions*. Clarendon Press, Oxford, 1987.
9. D. S. Stephenson, *Prog. NMR Spectrosc.*, 1989, **20**, 515.
10. G. L. Bretthorst, C.-C. Hung, D. A. D'Avignon, J. J. H. Ackerman, *J. Magn. Reson.*, 1988, **79**, 369.
11. D. L. Donoho, I. M. Johnstone, A. S. Stein and J. C. Hoch, *Proc. Natl Acad. Sci. USA*, 1990, **87**, 5066.
12. A. G. Redfield and R. K. Gupta, *Adv. Magn. Reson.*, 1971, **5**, 82.
13. J. D. Ellett Jr, M. G. Gibby, U. Haeberlen, L. M. Huber, M. Mehring, A. Pines and J. Waugh, *Adv. Magn. Reson.*, 1971, **5**, 117.
14. C.-N. Chen, D. I. Hoult and V. J. Sank, *J. Magn. Reson.*, 1983, **54**, 324.
15. A. Bax, *Two-Dimensional Nuclear Magnetic Resonance in Liquids*. Delft University Press, Delft, 1982.
16. J. Keeler and D. Neuhaus, *J. Magn. Reson.*, 1985, **63**, 454.
17. L. Müller and R. R. Ernst, *Mol. Phys.*, 1979, **38**, 963.
18. D. J. States, R. A. Haberkorn and D. J. Ruben, *J. Magn. Reson.*, 1982, **48**, 286.
19. G. Drobny, A. Pines, S. Sinton, D. Weitekamp and D. Wemmer, *Symp Faraday Soc.*, 1979, **13**, 49.
20. G. Bodenhausen, R. L. Vold and R. R. Vold, *J. Magn. Reson.*, 1980, **37**, 93.
21. D. Marion and K. Wüthrich, *Biochem. Biophys. Res. Commun.*, 1983, **113**, 967.
22. A. G. Palmer, J. Cavanagh, P. E. Wright and M. Rance, *J. Magn. Reson.*, 1991, **93**, 151.

23. J. Cavanagh and M. Rance, *J. Magn. Reson.*, 1990, **88**, 72.
24. J. Jeener, B. H. Meier, P. Bachmann and R. R. Ernst, *J. Chem. Phys.*, 1979, **71**, 4546.
25. L. Braunschweiler and R. R. Ernst, *J. Magn. Reson.*, 1983, **53**, 521.
26. A. Bax and D. G. Davis, *J. Magn. Reson.*, 1985, **65**, 355.
27. M. Rance, *J. Magn. Reson.*, 1987, **74**, 557.
28. R. Bazzo and I. D. Campbell, *J. Magn. Reson.*, 1988, **76**, 358.
29. O. W. Sørensen, G. W. Eich, M. H. Levitt, G. Bodenhausen and R. R. Ernst, *Prog. NMR Spectrosc.*, 1983, **16**, 163.
30. K. J. Packer and K. M. Wright, *Mol. Phys.*, 1983, **50**, 797.
31. F. J. M. van de Ven and C. W. Hilbers, *J. Magn. Reson.*, 1983, **54**, 512.
32. A. J. Shaka, J. Keeler, T. Frenkiel and R. Freeman, *J. Magn. Reson.*, 1983, **52**, 335.
33. A. J. Shaka, C. J. Lee and A. Pines, *J. Magn. Reson.*, 1988, **77**, 274.
34. J. Cavanagh, W. J. Chazin and M. Rance, *J. Magn. Reson.*, 1990, **87**, 110.
35. M. Rance and J. Cavanagh, *J. Magn. Reson.*, 1990, **87**, 363.
36. G. Otting, H. Widmer, G. Wagner and K. Wüthrich, *J. Magn. Reson.*, 1986, **66**, 187.
37. G. Wagner and K. Wüthrich, *J. Mol. Biol.*, 1982, **155**, 347.
38. J. S. Waugh, *J. Magn. Reson.*, 1986, **68**, 189.
39. A. Bax, *Isr. J. Chem.*, 1988, **28**, 309.
40. M. Kadkhodaie, O. Rivas, M. Tan, A. Mohebbi and A. J. Shaka, *J. Magn. Reson.*, 1991, **91**, 473.
41. J. Jeener, Ampère International Summer School, Basko Polje, Yugoslavia, 1971.
42. W. P. Aue, E. Bartholdi and R. R. Ernst, *J. Chem. Phys.*, 1976, **64**, 2229.
43. R. H. Griffey and A. G. Redfield, *Q. Rev. Biophys.*, 1987, **19**, 51.
44. G. Wagner, *Meth. Enzymol.*, 1989, **176**, 93.
45. D. C. Muchmore, L. P. McIntosh, C. B. Russell, D. E. Anderson and F. W. Dahlquist, *Meth. Enzymol.*, 1989, **177**, 44.
46. P. H. Bolton, *J. Magn. Reson.*, 1982, **48**, 336.
47. P. H. Bolton, *J. Magn. Reson.*, 1985, **62**, 143.
48. A. Bax, D. G. Davis and S. K. Sarkar, *J. Magn. Reson.*, 1985, **63**, 230.
49. L. Lerner and A. Bax, *J. Magn. Reson.*, 1986, **69**, 375.
50. M. Rance, P. E. Wright, B. A. Messerle and L. D. Field, *J. Am. Chem Soc.*, 1987, **109**, 1591.
51. N. R. Nirmala and G. Wagner, *J. Am. Chem Soc.*, 1988, **110**, 7557.
52. N. R. Nirmala and G. Wagner, *J. Magn. Reson.*, 1989, **82**, 659.
53. L. E. Kay, D. A. Torchia and A. Bax, *Biochemistry*, 1989, **28**, 8972.
54. G. Bodenhausen and D. J. Ruben, *Chem. Phys. Lett.*, 1980, **69**, 185.
55. M. R. Bendall, D. T. Pegg and D. M. Doddrell, *J. Magn. Reson.*, 1983, **52**, 81.
56. A. Bax, R. H. Griffey and B. L. Hawkins, *J. Magn. Reson.*, 1983, **55**, 301.
57. A. Bax, M. Ikura, L. E. Kay, D. A. Torchia and R. Tschudin, *J. Magn. Reson.*, 1990, **86**, 304.
58. (a) T. J. Norwood, J. Boyd, J. E. Heritage, N. Soffe and I. D. Campbell, *J. Magn. Reson.*, 1990, **87**, 488.
    (b) T. J. Norwood, J. Boyd and I. D. Campbell, *FEBS Lett.*, 1989, **255**, 369.
59. G. A. Morris and R. Freeman, *J. Am. Chem Soc.*, 1979, **101**, 760.
60. A. Bax, L. E. Kay, S. W. Sparks and D. A. Torchia, *J. Am. Chem Soc.*, 1989, **111**, 408.
61. (a) J. Glushka, M. Lee, S. Coffin and D. J. Cowburn, *J. Am. Chem Soc.*, 1989, **111**, 7716.
    (b) J. Glushka, M. Lee, S. Coffin and D. J. Cowburn, *J. Am. Chem Soc.*, 1990, **112**, 2843.
62. R. Richarz, K. Nagayama and K. Wüthrich, *Biochemistry*, 1980, **19**, 5189.
63. G. Wagner, *Q. Rev. Biophys.*, 1983, **16**, 1.
64. D. Brühweiler and G. Wagner, *J. Magn. Reson.*, 1986, **69**, 546.
65. J. Cavanagh, A. G. Palmer, P. E. Wright and M. Rance, *J. Magn. Reson.*, 1991, **91**, 429.
66. M. Rance and R. A. Byrd, *J. Magn. Reson.*, 1983, **54**, 221.
67. D. G. Davis, *J. Magn. Reson.*, 1989, **81**, 603.

68. G. M. Clore and A. M. Gronenborn, *Ann. Rev. Biophys. Biophys. Chem.*, 1991, **20**, 29.
69. L. E. Kay, D. Marion and A. Bax, *J. Magn. Reson.*, 1989, **84**, 72.
70. L. E. Kay, M. Ikura, R. Tschudin and A. Bax, *J. Magn. Reson.*, 1990, **89**, 496.
71. S. W. Fesik and E. R. P. Zuiderweg, *Q. Rev. Biophys.*, 1990, **23**, 97.
72. S. W. Fesik and E. R. P. Zuiderweg, *J. Magn. Reson.*, 1988, **78**, 588.
73. D. Marion, L. E. Kay, S. W. Sparks, D. A. Torchia and A. Bax, *J. Am. Chem Soc.*, 1989, **111**, 1515.
74. E. R. P. Zuiderweg and S. W. Fesik, *Biochemistry*, 1989, **28**, 2387.
75. A. G. Palmer, J. Cavanagh, R. A. Byrd and M. Rance, *J. Magn. Reson.*, 1992, **96**, 416.
76. J. Kördel, S. Forsen and W. J. Chazin, *Biochemistry*, 1989, **28**, 7065.
77. M. Karplus and J. A. McCammon, *Ann. Rev. Biochem.*, 1983, **53**, 263.
78. R. J. P. Williams, *Eur. J. Biochem.*, 1989, **183**, 479.
79. H. Frauenfelder, F. Parak and R. D. Young, *Ann. Rev. Biophys. Biophys. Chem.*, 1988, **17**, 451.
80. F. R. N. Gurd and T. M. Rothgeb, *Adv. Prot. Chem.*, 1979, **33**, 73.
81. T. M. G. Konong, R. Boelens, G. A. van de Marel, J. H. van Boom and R. Kaptein, *Biochemistry*, 1991, **30**, 3787.
82. J. E. Mertz, P. Güntert, K. Wüthrich and W. Braun, *J. Biomol. NMR*, 1991, **1**, 257.
83. H. Liu, P. D. Thomas and T. L. James, *J. Magn. Reson.*, 1992, **98**, 163.
84. A. Abragam, *Principles of Nuclear Magnetism*. Clarendon Press, Oxford, 1961.
85. R. E. London, *Meth. Enzymol.*, 1989, **176**, 358.
86. G. M. Clore, P. C. Driscoll, P. T. Wingfield and A. M. Gronenborn, *Biochemistry*, 1990, **29**, 7387.
87. J. Kördel, N. J. Skelton, M. Akke, A. G. Palmer and W. J. Chazin, *Biochemistry*, 1992, **31**, 4856.
88. A. G. Palmer, M. Rance and P. E. Wright, *J. Am. Chem. Soc.*, 1991, **113**, 4371.
89. J. W. Peng and G. Wagner, *J. Magn. Reson.*, 1992, **98**, 308.
90. D. M. Schneider, M. J. Dellwo and A. J. Wand, *Biochemistry*, 1992, **31**, 3645.
91. M. J. Stone, W. J. Fairbrother, A. G. Palmer, J. Reizer, M. H. Saier and P. E. Wright, *Biochemistry*, 1992, **31**, 4394.
92. A. G. Palmer, R. Hochstrasse, D. P. Millar, M. Rance and P. E.. Wright, *J. Amer. Chem. Soc.*, 1993 (in press).
93. J. W. Peng and G. Wagner, *Biochemistry*, 1992, **31**, 8571.
94. G. Barbato, M. Ikura, L. E. Kay, R. W. Pastore and A. Bax, *Biochemistry*, 1992, **31**, 5269.
95. L. K. Nicholson, L. E. Kay, D. M. Baldisseri, J. Arango, P. E. Young and D. A. Torchia, *Biochemistry*, 1992, **31**, 5253.
96. V. Sklenar, D. A. Torchia and A. Bax, *J. Magn. Reson.*, 1987, **73**, 375.
97. L. E. Kay, T. L. Jue, B. Bangerter and P. C. Demou, *J. Magn. Reson.*, 1987, **73**, 558.
98. L. E. Kay, L. K. Nicholson, F. Delagio, A. Bax and D. A. Torchia, *J. Magn. Reson.*, 1992, **97**, 359.
99. A. G. Palmer, N. J. Skelton, W. J. Chazin, P. E. Wright and M. Rance, *Mol. Phys.*, 1992, **75**, 699.
100. J. Boyd, U. Hommel and I. D. Campbell, *Chem. Phys. Lett.*, 1990, **175**, 477.
101. J. W. Peng, V. Thanabal and G. Wagner, *J. Magn. Reson.*, 1991, **95**, 421.
102. N. J. Skelton, A. G. Palmer, M. Akke, J. Kördel, M. Rance and W. J. Chazin, *J. Magn. Reson.*, in press, 1993.
103. S. Meiboom and D. Gill, *Rev. Sci. Instrum.*, 1958, **29**, 688.
104. H. Y. Carr and E. M. Purcell, *Phys. Rev.*, 1954, **94**, 630.
105. J. H. Noggle and R. E. Shirmer, *The Nuclear Overhauser Effect: Chemical Applications*. Academic Press, New York, 1971.
106. B. A. Messerle, G. Wider, G. Otting, C. Weber and K. Wüthrich, *J. Magn. Reson.*, 1989, **85**, 608.

107. R. L. Vold, R. R. Vold and H. E. Simon, *J. Magn. Reson.*, 1973, **11**, 283.
108. A. D. Bain, *J. Magn. Reson.*, 1984, **56**, 418.
109. G. Bodenhausen, H. Kogler and R. R. Ernst, *J. Magn. Reson.*, 1984, **58**, 370.
110. L. E. Kay, P. Keifer and T. Saarinen, *J. Am. Chem. Soc.*, 1992, **114**, 10 663.
111. J. C. Madsen and O. W. Sørensen, *J. Magn. Reson.*, 1992, **100**, 431.
112. A. Bax, A. F. Mehlkopf and J. Smidt, *J. Magn. Reson.*, 1979, **35**, 167.
113. F. Ni, *J. Magn. Reson.*, 1992, **100**, 391.